SCIENTIFIC REPORTS
nature research

Check for updates

OPEN

The dynamics of gas-bubble formation at saturated conditions in porous media flow

K. Alex Chang[1]✉ & W. Brent Lindquist[2]

We investigate the stability of gas bubbles formed at saturated (bubble-point) conditions during two-component (CO_2, H_2O), two-phase (gas, liquid) flow by developing and analyzing a 2 × 2 dynamical system describing flow through a single pore to study the dynamics of gas bubble formation and evolution. Our analysis indicates that three regimes occur at conditions pertinent to petroleum reservoirs. These regimes correspond to a critical point changing type from an unstable node to an unstable spiral and then to a stable spiral as flow rates increase. In the stable spiral case gas bubbles will achieve a steady-state finite size only if they form within the attractor region of the stable spiral. Otherwise, all gas bubbles that form undergo, possibly oscillatory, growth and then dissolve completely. Under steady flow conditions, this formation and dissolution repeats cyclically.

Compositional flow involving a dissolved gas is of importance in many areas, including oil reservoir production[3,14,22], pipeline transport[12,19,25,28], CO_2 sequestration[6,27], and the disposal of radioactive waste[4,5]. Such flow involves the inherent possibility of creation of a gas phase and its subsequent transport. Excluding specific tertiary recovery practices such as CO_2 foam flooding[24], keeping potential gas components dissolved in fluid phases is important for efficient extraction in reservoirs; the presence of gas bubbles and the resultant fluid–gas menisci complicates flow and can compete with fluid movement. The ability to prevent bubble formation through control of formation pressure or flow rates is therefore important for extraction efficiency.

Once formed in a porous medium, the gas phase is typically non-wetting. During imbibition (displacement by a wetting phase) a non-wetting phase can either exit pore space completely under piston-like displacement, or a fraction of it may become trapped in the form of one or more bubbles by a process known as snap-off. The snap-off process is strongly dependent on pore-geometry, wettability, viscosity and interfacial-tension conditions[26]. While snap-off is an important process in trapping the non-wetting phase, the process requires a starting condition in which both phases—non-wetting and wetting—are present.

In this study, we focus instead on the process by which a gas phase comes out of a saturated solution—forming bubbles. We therefore directly address the transition between single- and two-phase flow and the initial dynamics of those gas bubbles that do form. We are consequently studying flow conditions that would occur before sufficient (local) volumes of non-wetting phase have formed to begin any process of snap-off.

A challenge to the numerical simulation of compositional flow in porous media is the change in the system of equations that accompanies the appearance or disappearance of the gas phase. This difficulty has been addressed in several computational approaches[1,2,6–8,10,21]. In our computations of two-phase, two-component (H_2O, CO_2) flow in a 3D pore network[6], we noted the periodic appearance and dissolution of the gas phase in certain pores. Intensive evaluation of our algorithms led us to conclude that this observed cyclic phenomenon was not numerical in origin. In reviewing the literature on gas transport in porous media at reservoir scales[13], in micromodel studies[23], specific studies on gas bubble formation[17], and mathematical studies of gas phase disappearance in water-hydrogen systems[15], we have been unable to find any mention of this periodic phenomenon. We have therefore pursued a mathematical investigation. In this article, we extract a 2 × 2 dynamical system from the mathematical model upon which our computations in Chang and Lindquist[6] were based in order to study the dynamics of gas bubble formation and evolution and the mechanics of this phase-cycling phenomenon. We summarize the mathematical model and derive the dynamical system. We analyze the direction fields for this

[1]Department of Applied Mathematics, National Pingtung University, Pingtung, Taiwan, ROC. [2]Departments of Mathematics and Statistics and Geosciences, Texas Tech University, Lubbock, TX, USA. ✉email: chang@mail.nptu.edu.tw

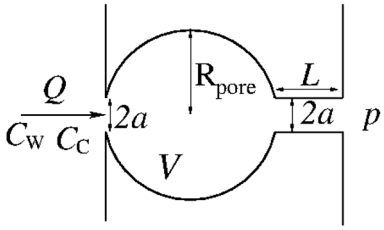

Figure 1. A cross section of the axially symmetric 3D geometry. The arrow indicating flow direction is placed on the axis of symmetry.

non-linear system, demonstrate the existence of critical points, and study solution trajectories. To support our analysis of the dynamical system, we obtain numerical solutions and conclude with a discussion of our results.

The mathematical model and the dynamical system

Here we summarize the model[6] in the context of flow through a single pore and develop the dynamical system.

The physical model. Consider a 3D, horizontal, axially symmetric network model consisting of a single spherical pore of radius R_{pore} and volume V (Fig. 1). The flow through the network is from left to right at the constant volumetric rate Q. The inflow solution is a liquid phase consisting of water with dissolved CO_2; the concentrations of H_2O and CO_2 in the solution are C_W and C_C, respectively.

The pore is initially filled with pure water. At the outlet, the pore is connected to a large reservoir of pure water held at pressure p. The length of the outlet channel is L and the radius of the cross section of the inlet and outlet channel is a. The system is held at constant temperature T.

The mathematical model. Under single-phase flow conditions (flow remains under-saturated with dissolved CO_2) the fluid transport is governed by the equations

$$V\frac{dC_W}{dt} = QC_W - C_W\Lambda_l(p_l - p), \qquad V\frac{dC_{Cl}}{dt} = QC_C - C_{Cl}\Lambda_l(p_l - p), \tag{1}$$

where C_{Cl} and p_l are, respectively, the concentration of CO_2 and the pressure of the liquid phase in the pore and Λ_l is the conductivity of the liquid phase from the pore to the outlet. The liquid phase is assumed incompressible with H_2O remaining the dominant species; therefore the concentration of water in the liquid phase is assumed to be the constant value $C_W = 1/18\,\text{mol cm}^{-3}$. Under these assumptions, the equations in (1) simplify to

$$p_l^{sp} = Q/\Lambda_l + p, \quad C_{Cl}(t) = C_C(1 - e^{-Qt/V}), \tag{2}$$

which provide the single-phase liquid pressure of the water and the CO_2 concentration in the pore.

A gas phase is generated in the pore when the concentration of CO_2 exceeds the solubility (see equation (17) of Chang and Lindquist[6]) of dissolved CO_2 in the liquid phase at the pressure p_l^{sp}, and the resulting two-phase flow follows the system below (these are, respectively, Eqs. (1), (9), (3), (4), (14) and (15) of Chang and Lindquist[6] applied to our single pore geometry):

$$s_l + s_g = 1, \tag{3a}$$

$$p_g = p_l + p_c, \tag{3b}$$

$$V\frac{dm_H}{dt} = \begin{cases} QC_W - Q_lC_W - Q_gC_{Hg}, & p_g > p, \\ QC_W - Q_lC_W, & p \geq p_g, \end{cases} \tag{4a}$$

$$V\frac{dm_C}{dt} = \begin{cases} QC_C - Q_lC_{Cl} - Q_gC_{Cg}, & p_g > p_l > p, \\ QC_C - Q_gC_{Cg}, & p_g > p \geq p_l, \\ QC_C, & p \geq p_g > p_l, \end{cases} \tag{4b}$$

$$\mu_{Hl}^{\ominus} + RT\ln\left(\frac{C_W}{C_W + C_{Cl}}\right) = \mu_{Hg}^{\ominus} + RT\ln\left(\frac{C_{Hg}RT}{p_H^*}\right), \tag{5a}$$

$$\mu_{Cl}^{\ominus} + RT\ln\left(\frac{C_{Cl}}{C_W + C_{Cl}}\right) = \mu_{Cg}^{\ominus} + RT\ln\left(\frac{C_{Cg}RT}{p_C^*}\right). \tag{5b}$$

In this system, s_l and s_g are the saturations of the liquid and gas phases; p_l and p_g are the pressures in the liquid and gas phase in the pore; C_{Hg} is the gas phase H_2O concentration; C_{Cl} and C_{Cg} are the liquid and gas phase CO_2 concentrations; m_H, m_C are the pore averaged concentrations of H_2O and CO_2,

$$m_{\mathrm{H}} = s_l C_{\mathrm{W}} + s_{\mathrm{g}} C_{\mathrm{Hg}}, \quad m_{\mathrm{C}} = s_l C_{\mathrm{Cl}} + s_{\mathrm{g}} C_{\mathrm{Cg}}; \tag{6}$$

and Q_l, Q_{g} are, respectively, the volumetric flow rates of the liquid and gas phases exiting the pore,

$$Q_l = \Lambda_l f(s_{\mathrm{g}})(p_l - p), \quad Q_{\mathrm{g}} = \Lambda_{\mathrm{g}} g(s_{\mathrm{g}})(p_{\mathrm{g}} - p). \tag{7}$$

In (7), $f(s_{\mathrm{g}})$ and $g(s_{\mathrm{g}})$ are the relative permeabilities of the liquid and gas phases respectively. As in Chang and Lindquist[6], we adopt the models[11]

$$f(s_{\mathrm{g}}) = \begin{cases} \frac{1}{2}(1-s_{\mathrm{g}})^2(2+s_{\mathrm{g}}), & p_l \geq p, \\ 1, & p_l < p, \end{cases} \qquad g(s_{\mathrm{g}}) = \begin{cases} s_{\mathrm{g}}^3, & p_{\mathrm{g}} \geq p, \\ 0, & p_{\mathrm{g}} < p. \end{cases} \tag{8}$$

Equations (4) and (8) are written to reflect the assumption that the outlet reservoir is sufficiently large that it can be assumed to remain pure water (i.e. any dissolved CO_2 in the outlet reservoir mixes to negligible concentration and exiting gas bubbles rise due to buoyancy and cannot flow back into the pore). Therefore, under the backflow condition, $p_l < p$, (4) and (8) reflect the fact that pure water flows into the pore from the outlet.

The variables Λ_l and Λ_{g} are the channel conductivities of the liquid and gas phase between the pore and the outlet reservoir. Conductivity values are modeled from the Hagen-Poiseuille equation, $\Lambda_l = \pi a^4/8\nu_l L$ and $\Lambda_{\mathrm{g}} = \pi a^4/8\nu_{\mathrm{g}} L$. The viscosities, ν_l and ν_{g}, of liquid and gas phases are given in units of Pa s by Lide and Kehiaian[18],

$$\ln(\nu_l) = -10.4349 - \frac{507.881}{(149.39 - T)},$$
$$\nu_{\mathrm{g}} = 4.6086 \times 10^{-8} T + 3.6436 \times 10^{-11} T^2 - 9.5765 \times 10^{-14} T^3 + 6.1091 \times 10^{-17} T^4,$$

over the temperature range $273.15\,^{\circ}\mathrm{K} \leq T \leq 373.15\,^{\circ}\mathrm{K}$.

Equations (5) express the equality (between the liquid and gas phases at equilibrium) of the chemical potentials of H_2O and CO_2. Inherent in our analysis is the assumption that phase changes occur rapidly compared to fluid transport so that equilibrium conditions are essentially maintained. $\mu^{\ominus}_{\beta l}$ and $\mu^{\ominus}_{\beta \mathrm{g}}$ are the chemical potentials of the species $\beta = H_2O$ or CO_2 in the liquid and gas phase at standard conditions. p^*_{H} and p^*_{C} are standard pressures which we take to be 1 bar. Equations (5) can be rewritten

$$C_{\mathrm{Hg}} RT = K_{\mathrm{H}} \frac{C_{\mathrm{W}}}{C_{\mathrm{W}} + C_{\mathrm{Cl}}}, \quad C_{\mathrm{Cg}} RT = K_{\mathrm{C}} \frac{C_{\mathrm{Cl}}}{C_{\mathrm{W}} + C_{\mathrm{Cl}}}, \tag{9}$$

where

$$K_{\mathrm{H}}(T) = p^*_{\mathrm{H}} \exp[(\mu^{\ominus}_{\mathrm{Hl}} - \mu^{\ominus}_{\mathrm{Hg}})/RT], \qquad K_{\mathrm{C}}(T) = p^*_{\mathrm{C}} \exp[(\mu^{\ominus}_{\mathrm{Cl}} - \mu^{\ominus}_{\mathrm{Cg}})/RT].$$

Over the range of temperatures of interest, $[273.15\,^{\circ}\mathrm{K}, 373.15\,^{\circ}\mathrm{K}]$, $K_{\mathrm{H}}(T)$ lies in the range $[1.82864 \times 10^{-5}, 1.94313 \times 10^{-5}]$ and the ratio $K_{\mathrm{H}}(T)/K_{\mathrm{C}}(T)$ is in the range $[5.76231 \times 10^{-4}, 4.25324 \times 10^{-3}]$.

Assuming the liquid phase is perfectly wetting, the capillary pressure in (3b) is modeled by the Young–Laplace equation,

$$p_c = \frac{2\gamma}{r}, \tag{10}$$

where γ is the surface tension and r is the radius of the gas bubble. We assume that the gas phase forms as a single bubble in the pore and therefore estimate $r = s_{\mathrm{g}}^{1/3} \mathrm{R}_{\mathrm{pore}}$. The surface tension, γ, is evaluated by the Eötvös rule,

$$\gamma C_{\mathrm{W}}^{-2/3} = \begin{cases} \kappa(T_c - T), & T \leq T_c, \\ 0, & T > T_c, \end{cases}$$

where $T_c = 647^{\circ} K$ is the critical temperature for water and $\kappa = 2.1 \times 10^{-7}\ \mathrm{JK^{-1}mol^{-2/3}}$. We also assume the gas phase is ideal; therefore the total pressure of the gas phase is

$$p_{\mathrm{g}} = C_{\mathrm{Cg}} RT + C_{\mathrm{Hg}} RT. \tag{11}$$

The dynamical system. It will be convenient to divide concentration variables by C_{W}, pressure variables by $C_{\mathrm{W}} RT$, flow rates by V, and denote the resultant variables using "over-bar" notation (e.g. $\overline{C}_{\mathrm{Cl}} = C_{\mathrm{Cl}}/C_{\mathrm{W}}$, $\overline{m}_{\mathrm{H}} = m_{\mathrm{H}}/C_{\mathrm{W}}$, $\overline{p} = p/C_{\mathrm{W}} RT$, $\overline{K}_{\mathrm{C}} = K_{\mathrm{C}}/C_{\mathrm{W}} RT$, $\overline{Q} = Q/V$). As a result, all variables become dimensionless except for the volumetric flow rates, $\overline{Q}$, $\overline{Q}_l$, $\overline{Q}_{\mathrm{g}}$, which have dimension of time^{-1}. The natural time variable (through which to introduce dimensionless flow rates) is the quantity $\overline{Q}^{-1}$. However, the flow rate $\overline{Q}$ will be a critical variable in our analysis. We therefore retain the variable $\overline{Q}$ in our equations and consequently keep an explicit non-dimensional time variable in the dynamical system.

We identify the fundamental variables, w, y, of the dynamical system as

$$w = \overline{C}_{\mathrm{Cg}}, \quad 0 \leq w \leq \frac{\overline{K}_{\mathrm{C}} \overline{C}_{\mathrm{C}}}{1 + \overline{C}_{\mathrm{C}}} \stackrel{\mathrm{def}}{=} \overline{C}_{\mathrm{Cg}}(\overline{C}_{\mathrm{C}}); \qquad y = s_{\mathrm{g}}, \quad 0 \leq y \leq 1. \tag{12}$$

Since the inlet solution is an aqueous phase, we require $\overline{C}_C < 1$. Therefore $w \le \overline{C}_{Cg}(\overline{C}_C) < \overline{K}_C$. From (9), the concentrations $\overline{C}_{Hg}$ and $\overline{C}_{Cl}$ can be expressed in terms of w:

$$\begin{aligned} \overline{C}_{Hg} &= \overline{K}_H \frac{\overline{K}_C - w}{\overline{K}_C}, \qquad \overline{C}_{Hg} \in \left[\frac{\overline{K}_H}{1+\overline{C}_C}, \overline{K}_H\right]; \\ \overline{C}_{Cl} &= \frac{w}{\overline{K}_C - w}, \qquad \overline{C}_{Cl} \in [0, \overline{C}_C]. \end{aligned} \tag{13}$$

Note that the definition of $\overline{C}_{Cg}(\overline{C}_C)$ in (12) and the relation for $\overline{C}_{Cl}$ in (13) gives the identity $\overline{C}_C = \overline{C}_{Cg}(\overline{C}_C)/(\overline{K}_C - \overline{C}_{Cg}(\overline{C}_C)) = \overline{C}_{Cl}(\overline{C}_{Cg}(\overline{C}_C))$.

From (10), (11) and (3b), the dimensionless pore phase pressures are expressed in terms of w and y as

$$\begin{aligned} \overline{p}_c &= \bar{s} y^{-1/3}, \quad \overline{p}_g = \left(1 - \frac{\overline{K}_H}{\overline{K}_C}\right) w + \overline{K}_H, \\ \overline{p}_l &= \left(1 - \frac{\overline{K}_H}{\overline{K}_C}\right) w + \overline{K}_H - \bar{s} y^{-1/3}, \end{aligned} \tag{14}$$

where we have defined $\bar{s} = 2\gamma/(R_{pore} C_W RT)$. From (14) we note $\overline{p}_l < \overline{p}_g$. Equations (4) become

$$\begin{aligned} \frac{d\overline{m}_H}{dt} &= \left\{ \begin{array}{ll} \overline{Q} - \overline{Q}_l(w,y) - \overline{C}_{Hg}(w)\overline{Q}_g(w,y), & \overline{p}_g > \overline{p}, \\ \overline{Q} - \overline{Q}_l(w,y), & \overline{p} \ge \overline{p}_g, \end{array} \right\} \\ &\stackrel{\text{def}}{=} \Delta_H(w,y), \end{aligned} \tag{15a}$$

$$\begin{aligned} \frac{d\overline{m}_C}{dt} &= \left\{ \begin{array}{ll} \overline{C}_C\overline{Q} - \overline{C}_{Cl}(w)\overline{Q}_l(w,y) - w\overline{Q}_g(w,y), & \overline{p}_g > \overline{p}_l > \overline{p}, \\ \overline{C}_C\overline{Q} - w\overline{Q}_g(w,y), & \overline{p}_g > \overline{p} \ge \overline{p}_l, \\ \overline{C}_C\overline{Q}, & \overline{p} \ge \overline{p}_g > \overline{p}_l, \end{array} \right\} \\ &\stackrel{\text{def}}{=} \Delta_C(w,y). \end{aligned} \tag{15b}$$

We can obtain alternate expressions to (15) for Δ_H and Δ_C. Starting from (6), we have

$$\overline{m}_H(w,y) = 1 - y + y\overline{C}_{Hg}(w), \quad \overline{m}_C(w,y) = (1-y)\overline{C}_{Cl}(w) + yw. \tag{16}$$

Taking the time derivative of (16) gives the alternate expressions,

$$\begin{aligned} \Delta_H(w,y) &= y\frac{d\overline{C}_{Hg}(w)}{dw}\frac{dw}{dt} + (\overline{C}_{Hg}(w) - 1)\frac{dy}{dt} \\ &\stackrel{\text{def}}{=} G_1(w,y)\frac{dw}{dt} + G_2(w)\frac{dy}{dt}, \end{aligned} \tag{17a}$$

$$\begin{aligned} \Delta_C(w,y) &= \left[(1-y)\frac{d\overline{C}_{Cl}(w)}{dw} + y\right]\frac{dw}{dt} + (w - \overline{C}_{Cl}(w))\frac{dy}{dt} \\ &\stackrel{\text{def}}{=} F_1(w,y)\frac{dw}{dt} + F_2(w)\frac{dy}{dt}, \end{aligned} \tag{17b}$$

where for notational brevity, we have introduced the functions G_1, G_2, F_1, F_2. Solving (17) for dw/dt and dy/dt gives the dynamical system

$$\begin{aligned} \frac{dw}{dt} &= \frac{\Delta_C(w,y)G_2(w) - F_2(w)\Delta_H(w,y)}{F_1(w,y)G_2(w) - F_2(w)G_1(w,y)}, \\ \frac{dy}{dt} &= \frac{F_1(w,y)\Delta_H(w,y) - \Delta_C(w,y)G_1(w,y)}{F_1(w,y)G_2(w) - F_2(w)G_1(w,y)}. \end{aligned} \tag{18}$$

Using (13) to evaluate the concentrations and concentration derivatives in (17) and noting that $\overline{K}_H < 2 \times 10^{-5}$ and $\overline{K}_H/\overline{K}_C < O(10^{-3})$ over the range of temperatures of interest, we have, to good approximation,

$$\overline{C}_{Hg}(w) \approx 0 \Rightarrow G_2(w) \approx -1; \qquad \frac{d\overline{C}_{Hg}(w)}{dw} = -\frac{\overline{K}_H}{\overline{K}_C} \approx 0 \Rightarrow G_1(w,y) \approx 0. \tag{19}$$

The statement $\overline{K}_H/\overline{K}_C \ll 1$ has a physical consequence, namely that the H_2O component in the gas phase remains small in comparison to the CO_2 component. Approximations (19) imply the simplifications: of (14) to

$$\overline{p}_c(y) = \bar{s} y^{-1/3}, \qquad \overline{p}_g(w) \approx w, \qquad \overline{p}_l(w,y) \approx w - \bar{s} y^{-1/3}; \tag{14'}$$

of (15) to

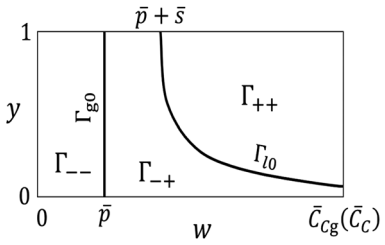

Figure 2. The phase space is divided into three regions, Γ_{++}, Γ_{-+} and Γ_{--}, by the curves Γ_{l0} and Γ_{g0}.

$$\Delta_H(w,y) \approx \overline{Q} - \overline{Q}_l(w,y), \tag{15'a}$$

$$\Delta_C(w,y) = \begin{cases} \overline{C}_C\overline{Q} - \overline{C}_{Cl}(w)\overline{Q}_l(w,y) - w\overline{Q}_g(w,y), & \overline{p}_g(w) > \overline{p}_l(w,y) > \overline{p}, \\ \overline{C}_C\overline{Q} - w\overline{Q}_g(w,y), & \overline{p}_g(w) > \overline{p} \geq \overline{p}_l(w,y), \\ \overline{C}_C\overline{Q}, & \overline{p} \geq \overline{p}_g(w) > \overline{p}_l(w,y); \end{cases} \tag{15'b}$$

and of (18) to

$$\frac{dw}{dt} \approx \frac{F_2(w)\Delta_H(w,y) + \Delta_C(w,y)}{F_1(w,y)} \stackrel{\text{def}}{=} F(w,y), \quad \frac{dy}{dt} \approx -\Delta_H(w,y) \stackrel{\text{def}}{=} G(w,y). \tag{18'}$$

The second and third equations of (14′) hold only for $w \gg \overline{K}_H = O(10^{-5})$. This approximation will ultimately effect computation of phase space trajectories for values of $w \lesssim 10^{-4}$. Our results will demonstrate that the region of phase space governing bubble formation occurs well away from "small w" values, and we proceed with the approximation (14′).

In (18′) we have used a standard notation, $F(w, y)$ and $G(w, y)$, for the right-hand side of this two-by-two system of ODEs. The dynamical system we consider is (18′) with: Δ_H, Δ_C defined by (15′); F_1, F_2 defined by (17b); $\overline{Q}_l$, $\overline{Q}_g$ given by (7) and (8) appropriately normalized,

$$\overline{Q}_l(w,y) = \begin{cases} \overline{\Lambda}_l f(y)(\overline{p}_l(w,y) - \overline{p}), & \overline{p}_l(w,y) > \overline{p}, \\ 0, & \overline{p}_l(w,y) = \overline{p}, \\ \overline{\Lambda}_l(\overline{p}_l(w,y) - \overline{p}), & \overline{p}_l(w,y) < \overline{p}, \end{cases} \tag{7'a}$$

$$\overline{Q}_g(w,y) = \begin{cases} \overline{\Lambda}_g g(y)(\overline{p}_g(w) - \overline{p}), & \overline{p}_g(w) > \overline{p}, \\ 0, & \overline{p}_g(w) \leq \overline{p}, \end{cases} \tag{7'b}$$

where $\overline{\Lambda}_\alpha = \Lambda_\alpha C_W RT/V, \alpha = l,\ g$; and the phase pressures given by (14′).

Analysis of the dynamical system

The curves $\overline{Q}_l = 0$ and $\overline{Q}_g = 0$. The physical w, y phase space for (18′) is $0 \leq w \leq \overline{C}_{Cg}(\overline{C}_C)$, $0 < y \leq 1$. It contains two important curves. The first is the curve Γ_{l0} defined by the condition $\overline{Q}_l(w,y) = \overline{p}_l(w,y) - \overline{p} = 0$ which, from (14′), can be written either as

$$y_{l0}(w) = (\bar{s}/(w-\overline{p}))^3 \qquad \text{or} \qquad w_{l0}(y) = \overline{p} + \bar{s}/y^{1/3}. \tag{20}$$

From (20), $w_{l0}(1) = \overline{p} + \bar{s}$. Note that, for any point $(w,y) \in [0, \overline{C}_{Cg}(\overline{C}_C)] \times (0,1]$ on Γ_{l0}, we have $\overline{C}_{Cg}(\overline{C}_C) \geq \overline{p}_g = \overline{p} + \bar{s}y^{-1/3} > \overline{p} + \bar{s}$, by which we confirm that the value $\overline{p} + \bar{s}$ lies strictly in the range $0 < \overline{p} + \bar{s} < \overline{C}_{Cg}(\overline{C}_C)$. Thus, $0 < y_{l0}(w) \leq 1$ for all $w \in [\overline{p} + \bar{s}, \overline{C}_{Cg}(\overline{C}_C)]$. Furthermore, from (20) we note that the slope $dy_{l0}(w)/dw < 0$ for $w \in [\overline{p} + \bar{s}, \overline{C}_{Cg}(\overline{C}_C)]$. Thus $y_{l0}(w)$ decreases from its maximum value $y_{l0}(\overline{p} + \bar{s}) = 1$ over the domain $[\overline{p} + \bar{s}, \overline{C}_{Cg}(\overline{C}_C)]$. At the $w = \overline{C}_{Cg}(\overline{C}_C)$ endpoint of Γ_{l0} we have

$$1 > y_{l0}(\overline{C}_{Cg}(\overline{C}_C)) = \left(\frac{\bar{s}}{\overline{C}_{Cg}(\overline{C}_C) - \overline{p}}\right)^3 > 0.$$

The second important curve in the phase space, Γ_{g0}, is defined by

$$\overline{Q}_g = \overline{p}_g(w) - \overline{p} = w - \overline{p} = 0; \tag{21}$$

i.e., Γ_{g0} is the vertical line $w = \overline{p}$.

The curves Γ_{l0} and Γ_{g0} divide the phase space into three regions. Let: Γ_{++} denote the region of the phase space where $\overline{p}_g(w) > \overline{p}_l(w,y) > \overline{p}$; Γ_{-+} denote the region where $\overline{p}_g(w) > \overline{p} > \overline{p}_l(w,y)$; and Γ_{--} denote the region where $\overline{p} > \overline{p}_g(w) > \overline{p}_l(w,y)$. Figure 2 provides sketches of Γ_{l0}, Γ_{g0} and indicates the regions Γ_{++}, Γ_{-+} and Γ_{--}.

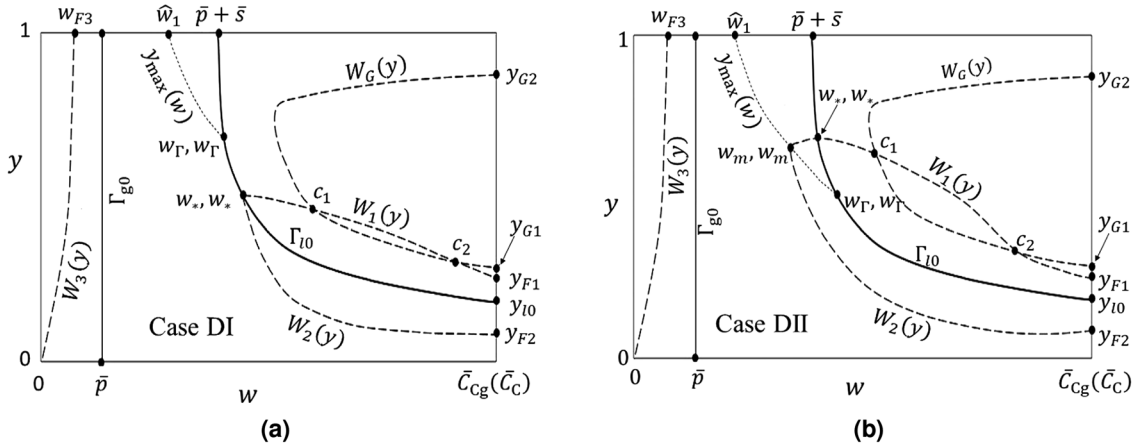

Figure 3. Sketch of the relevant phase space curves and regions discussed in the text and Appendices A to E in the supplementary material. The difference in the curve $W_2(y)$ in cases DI and DII is discussed in Appendix D.

Direction fields. As the dynamical system (18′) is complex and the details of its analysis are not straightforward, to respect article length we have relegated most of these details to a series of appendices in the accompanying supplementary material. The manuscript text references the appropriate appendix as needed.

The direction field $dy/dt = G(w, y)$. The direction field dy/dt is analyzed in Appendix A of the supplementary material by considering the isoclines of $G(w, y)$. All isoclines in the region $\Gamma_{--} \cup \Gamma_{g0} \cup \Gamma_{-+} \cup \Gamma_{l0}$ are of the monotonic form (A.9) given in Appendix A and are negative-valued. The curve Γ_{g0} is not an isocline; explicit evaluation using (18′), (15′a), (7′a), (3b), (21) and (14′) gives $G(\bar{p}, y) = -\overline{\Lambda}_l \bar{s} y^{-1/3} - \overline{Q} < 0$. From (18′) and (15′a) it is straightforward to see that Γ_{l0} is the $G(w, y) = -\overline{Q}$ isocline.

The $G(w, y)$ isoclines in Γ_{++} have the form (A.4) of Appendix A and are "concave-up" in the direction $w \to \infty$ (see Fig. A.1(a) of Appendix A). The only region where $G(w, y)$ can take positive values (implying gas bubble growth) is Γ_{++}.

There exists a maximum value of $\overline{Q}$ such that, for flow strengths above this value, the isocline $G(w, y) = 0$ does not (and hence no positive-valued isoclines can) appear in the physical phase space and no gas bubble growth is possible. Computation for this maximum flow strength $\overline{Q}_{\max} = \alpha_{\max} \overline{\Lambda}_l \bar{s}$, is illustrated in Fig. A.1(b) of Appendix A. With the condition $\overline{Q} < \overline{Q}_{\max}$ satisfied, the form of the isocline $G(w, y) = 0$ is shown in Fig. 3 where, following the notation introduced in Appendix A, it is referred to as $W_G(y)$. $W_G(y)$ intersects the phase space boundary $w = \overline{C}_{\mathrm{Cg}}(\overline{C}_{\mathrm{C}})$ at the values y_{G1} and y_{G2}.

The direction field $dw/dt = F(w, y)$. The direction field $F(w, y)$ is more complex and we have relied on estimation procedures to determine its behavior. To proceed, we express $F(w, y)$ in (18′) as

$$F(w,y) = \frac{(\overline{K}_{\mathrm{C}} - w)[F_2(w)\Delta_{\mathrm{H}}(\mathrm{w},\mathrm{y}) + \Delta_{\mathrm{C}}(\mathrm{w},\mathrm{y})]}{(\overline{K}_{\mathrm{C}} - w)F_1(w,y)} \stackrel{\mathrm{def}}{=} \frac{\widetilde{F}(w,y)}{(\overline{K}_{\mathrm{C}} - w)F_1(w,y)}. \tag{22}$$

Since the denominator in (22) is always positive, we note that F and $\widetilde{F}$ have the same zero-points and signs. Using (15′), and (7′) we obtain the following expressions for $\widetilde{F}$:

$$\begin{aligned}\widetilde{F}(w,y)|_{\Gamma_{++}} = (\overline{K}_{\mathrm{C}} - w)\{&(F_2(w) + \overline{C}_{\mathrm{C}})\overline{Q} - w[\overline{\Lambda}_l f(y) + \overline{\Lambda}_{\mathrm{g}} g(y)](w - \bar{p}) \\ &+ w\overline{\Lambda}_l f(y)\bar{s}y^{-1/3}\};\end{aligned} \tag{23a}$$

$$\widetilde{F}(w,y)|_{\Gamma_{l0}} = (\overline{K}_{\mathrm{C}} - w)\{(F_2(w) + \overline{C}_{\mathrm{C}})\overline{Q} - w\overline{\Lambda}_{\mathrm{g}}\bar{s}y_{l0}^{8/3}\}; \tag{23b}$$

$$\begin{aligned}\widetilde{F}(w,y)|_{\Gamma_{-+}} = (\overline{K}_{\mathrm{C}} - w)\{&(F_2(w) + \overline{C}_{\mathrm{C}})\overline{Q} - [F_2(w)\overline{\Lambda}_l + w\overline{\Lambda}_{\mathrm{g}} y^3](w - \bar{p}) \\ &+ F_2(w)\overline{\Lambda}_l \bar{s}y^{-1/3}\};\end{aligned} \tag{23c}$$

$$\widetilde{F}(w,y)|_{\Gamma_{\mathrm{g0}}} = (\overline{K}_{\mathrm{C}} - \bar{p})\{(F_2(\bar{p}) + \overline{C}_{\mathrm{C}})\overline{Q} + F_2(\bar{p})\overline{\Lambda}_l \bar{s}y^{-1/3}\}; \tag{23d}$$

$$\begin{aligned}\widetilde{F}(w,y)|_{\Gamma_{--}} = (\overline{K}_{\mathrm{C}} - w)\{&(F_2(w) + \overline{C}_{\mathrm{C}})\overline{Q} - F_2(w)\overline{\Lambda}_l(w - \bar{p}) \\ &+ F_2(w)\overline{\Lambda}_l \bar{s}y^{-1/3}\};\end{aligned} \tag{23e}$$

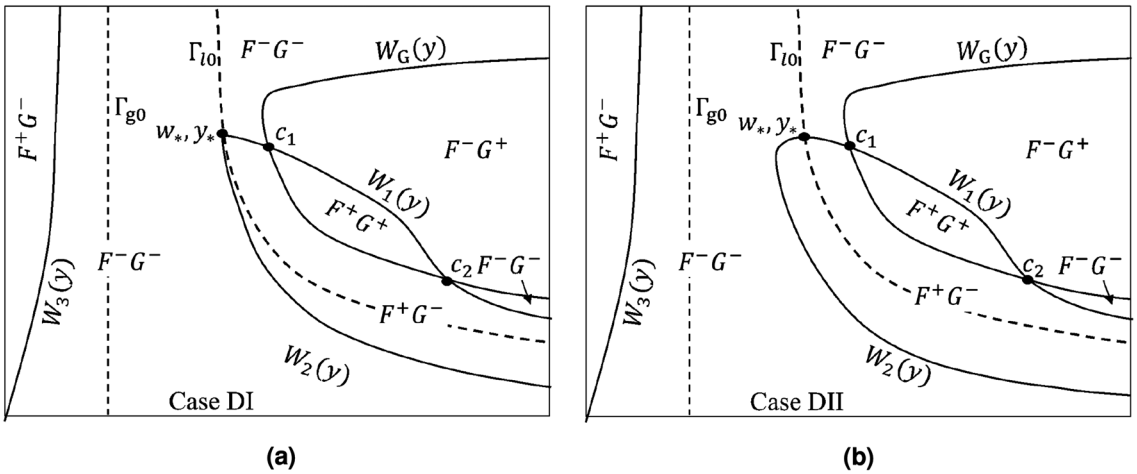

Figure 4. Signs for the direction fields $F(w, y)$, $G(w, y)$ in the phase space for (**a**) Case DI and (**b**) Case DII. F^+G^- denotes a region where $F(w, y) > 0, G(w, y) < 0$, etc.

where by (17b) and (13), $F_2(w) = w - w/(\overline{K}_C - w)$. Note $F_2(w) < 0$ providing $\overline{K}_C < 1$, which is indeed the case in our numerical computations (see Table 1). However, $F_2(w) + \overline{C}_C > 0$ in the domain of interest. The expressions for $\widetilde{F}(w, y)$ in (23) are continuous across the curves Γ_{l0} and Γ_{g0}.

We introduce four restrictions on the range of $\overline{Q}$ to make our estimations tractable. Evaluating (23b) at the point $(\overline{p} + \overline{s}, 1)$, we have

$$\widetilde{F}(\overline{p} + \overline{s}, 1) = (\overline{K}_C - \overline{p} - \overline{s})\left[F_2(\overline{p} + \overline{s}) + \overline{C}_C\right]\left\{\overline{Q} - \frac{(\overline{p} + \overline{s})\overline{\Lambda}_g\overline{s}}{\left[F_2(\overline{p} + \overline{s}) + \overline{C}_C\right]}\right\}.$$

Restricting $\overline{Q} < (\overline{p} + \overline{s})\overline{\Lambda}_g\overline{s}/\left[F_2(\overline{p} + \overline{s}) + \overline{C}_C\right]$ will guarantee that $\widetilde{F}(\overline{p} + \overline{s}, 1) < 0$. Evaluating (23b) at the point $(\overline{C}_{Cg}(\overline{C}_C), y_{l0}(\overline{C}_{Cg}(\overline{C}_C)))$, we have

$$\widetilde{F}(\overline{C}_{Cg}(\overline{C}_C), y_{l0}(\overline{C}_{Cg}(\overline{C}_C))) = (\overline{K}_C - \overline{C}_{Cg}(\overline{C}_C))\overline{C}_{Cg}(\overline{C}_C)\left\{\overline{Q} - \overline{\Lambda}_g\overline{s}\left(\frac{\overline{s}}{\overline{C}_{Cg}(\overline{C}_C) - \overline{p}}\right)^8\right\}.$$

Restricting $\overline{Q} > \overline{\Lambda}_g\overline{s}\left[\overline{s}/(\overline{C}_{Cg}(\overline{C}_C) - \overline{p})\right]^8$ will guarantee that $\widetilde{F}(\overline{C}_{Cg}(\overline{C}_C), y_{l0}(\overline{C}_{Cg}(\overline{C}_C))) > 0$. Evaluating (23d) at the point $(\overline{p}, 1)$ we have

$$\widetilde{F}(\overline{p}, 1) = (\overline{K}_C - \overline{p})\left\{(F_2(\overline{p}) + \overline{C}_C)\overline{Q} + F_2(\overline{p})\overline{\Lambda}_l\overline{s}\right\}.$$

Restricting $\overline{Q} < -F_2(\overline{p})\overline{\Lambda}_l\overline{s}/(F_2(\overline{p}) + \overline{C}_C)$ will guarantee that $\widetilde{F}(\overline{p}, 1) < 0$. We also note from the previous section that the restriction $\overline{Q} < \overline{Q}_{max}$ guarantees that there is a region $G(w, y) > 0$ within Γ_{++}. We combine these restrictions on $\overline{Q}$ into the single statement,

$$\left(\frac{\overline{s}}{\overline{C}_{Cg}(\overline{C}_C) - \overline{p}}\right)^8 < \frac{\overline{Q}}{\overline{\Lambda}_g\overline{s}} < \min\left(\frac{\overline{p} + \overline{s}}{F_2(\overline{p} + \overline{s}) + \overline{C}_C}, \frac{-\overline{\Lambda}_l F_2(\overline{p})}{\overline{\Lambda}_g(F_2(\overline{p}) + \overline{C}_C)}, \alpha_{max}\frac{\overline{\Lambda}_l}{\overline{\Lambda}_g}\right). \tag{24}$$

The behavior of $\widetilde{F}(w, y)$ in the phase space is discussed next.

$\widetilde{F}(w, y)$ on Γ_{l0}. In Appendix B (supplementary material) we show $\widetilde{F}(w, y)$ has the following behavior on Γ_{l0}:

$$\widetilde{F}(w, y)|_{\Gamma_{l0}}\begin{cases} < 0, & w \in [\overline{p} + \overline{s}, w_*), \\ = 0, & w = w_*, \\ > 0, & w \in (w_*, \overline{C}_{Cg}(\overline{C}_C)]. \end{cases} \tag{B.9}$$

The existence of the point $(w_*, y_* = y_{l0}(w_*))$ within the physical domain is guaranteed by assumption (24). The point (w_*, y_*) is illustrated in Fig. 3.

$\widetilde{F}(w, y)$ on Γ_{g0}. Using (23d) we see that the derivative $\partial\widetilde{F}(\overline{p}, y))/\partial y = -F_2(\overline{p})(\overline{K}_C - \overline{p})\overline{\Lambda}_l\overline{s}y^{-4/3}/3 > 0$. Hence $\widetilde{F}(\overline{p}, y)$ is a strictly increasing function of y. From restriction (24) we have $\widetilde{F}(\overline{p}, 1) < 0$. Therefore, $\widetilde{F}(\overline{p}, y) < 0$ for all $y \in (0, 1]$.

$\widetilde{F}(w, y)$ in Γ_{++}. $\widetilde{F}(w, y)|_{\Gamma_{++}}$ is analyzed in Appendix C (supplementary material). There we prove the existence of a single curve segment, $W_1(y)$, in Γ_{++} on which $\widetilde{F}(w, y)|_{\Gamma_{++}} = 0$. $W_1(y)$ connects the point (w_*, y_*) on Γ_{l0} to a point $(\overline{C}_{Cg}(\overline{C}_C), y_{F1})$ where y_{F1} lies in the interval $(y_{l0}(\overline{C}_{Cg}(\overline{C}_C)), y_{G1})$. By Lemma C of Appendix C,

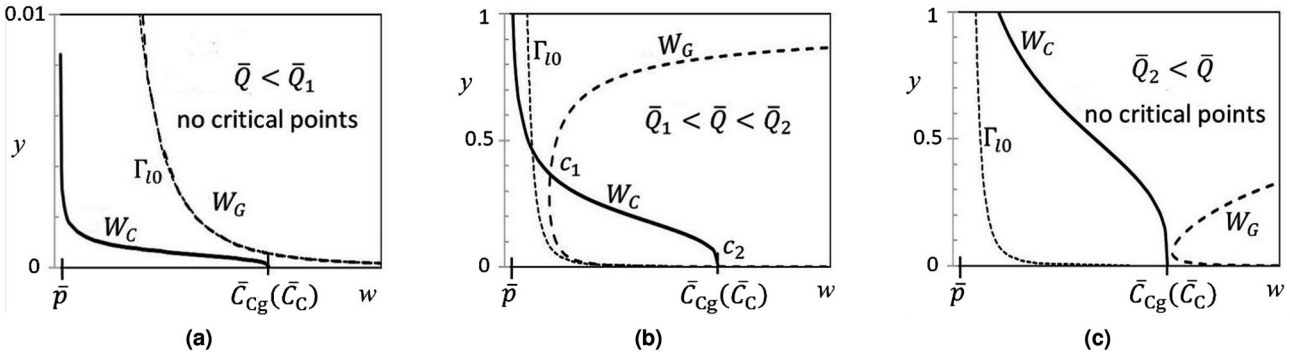

Figure 5. Sketches of the curves W_C and W_G for values of $\bar{Q}$ in the three ranges (**a**) $\bar{Q} < \bar{Q}_1$; (**b**) $\bar{Q} \in (\bar{Q}_1, \bar{Q}_2)$ and (**c**) $\bar{Q}_2 < \bar{Q}$. In (**a**), for clarity, only a subset of the y-axis range is shown. Note that W_G approaches very close to, but always lies above, the curve Γ_{l0}.

$y_{F1} < y_*$. $W_1(y)$ is a continuous function of y; for each value of $y \in [y_{F1}, y_*]$ there is a unique value $W_1(y)$. A sketch of this curve segment is shown in Fig. 3. Regions where $\widetilde{F}(w,y)|_{\Gamma_{++}} \gtrless 0$ are indicated in Fig. 4.

$\widetilde{F}(w,y)$ in Γ_{-+}. $\widetilde{F}(w,y)|_{\Gamma_{-+}}$ is analyzed in Appendix D (supplementary material). There we show Γ_{-+} contains a curve, $y_{\max}(w)$, on which $\partial \widetilde{F}(w,y)/\partial y|_{\Gamma_{-+}} = 0$. $y_{\max}(w)$ joins a unique point $(\widehat{w}_1, 1)$, where $\bar{p} < \widehat{w}_1 < \bar{p} + \bar{s}$, to a unique point (w_Γ, y_Γ) on Γ_{l0}. In addition, $\widetilde{F}(w,y)|_{\Gamma_{-+}} = 0$ in Γ_{-+} on a single curve segment $W_2(y)$ joining the point (w_*, y_*) to $(\bar{C}_{Cg}(\bar{C}_C), y_{F2})$, where y_{F2} is a unique value satisfying $0 < y_{F2} < y_{l0}(\bar{C}_{Cg}(\bar{C}_C))$. The curve $W_2(y)$ can have two possible forms, depending on the relative size of w_Γ and w_* (cases DI and DII in Appendix D). The curves $y_{\max}(w)$ and $W_2(y)$ are sketched in Fig. 3 and the points $(\widehat{w}_1, 1)$, (w_Γ, y_Γ) and $(\bar{C}_{Cg}(\bar{C}_C), y_{F2})$ are indicated. Regions where $\widetilde{F}(w,y)|_{\Gamma_{-+}} \gtrless 0$ are shown in Fig. 4.

$\widetilde{F}(w,y)$ in Γ_{--}. The function $\widetilde{F}(w,y)|_{\Gamma_{--}}$ is analyzed in Appendix E (supplementary material). On the boundary $y = 1$ there exists a unique value $w_{F3} \in (0, \bar{p})$ such that $\widetilde{F}(w_{F3}, 1) = 0$. In the interior of Γ_{--}, $\widetilde{F}(w,y)|_{\Gamma_{--}} = 0$ only on a curve $W_3(y)$ having the properties: $\lim_{y\to 0^+} W_3(y) \to 0$, $W_3(1) = w_{F3}$, and $dW_3(y)/dy > 0$. Fig. 3 shows a sketch of the curve $W_3(y)$ and the point $(w_{F3}, 1)$. Regions where $\widetilde{F}(w,y)|_{\Gamma_{--}} \gtrless 0$ are indicated in Fig. 4.

Critical point existence. A point (w_c, y_c) is a critical point of (18′) if $F(w_c, y_c) = G(w_c, y_c) = 0$. From (18′), we conclude (w_c, y_c) is a critical point of (18′) iff $\Delta_H(w_c, y_c) = \Delta_C(w_c, y_c) = 0$. From (18′), the equation $\Delta_H(w, y) = 0$ defines the isocline $G(w,y) = 0$, i.e. the curve W_G. Similarly the equation $\Delta_C(w, y) = 0$ implicitly defines a curve W_F. Thus (w_c, y_c) is a critical point iff it is a crossing point of the curves W_G and W_F.

The curve W_F is complicated to analyze. However, examining (15′b) in Γ_{++} we recognize that the curve W_C defined by the equation

$$\Delta'_C(w,y) = (\bar{C}_C - \bar{C}_{Cl}(w))\bar{Q} - w\bar{Q}_g(w,y) = 0, \tag{25}$$

also crosses the curve W_G at exactly the same critical points. Equation (25) can be explicitly solved for $y|_{W_C}$,

$$(y|_{W_C})^3 = \left(\bar{C}_C - \frac{w}{\bar{K}_C - w}\right)\frac{1}{w(w-\bar{p})}\frac{\bar{Q}}{\bar{\Lambda}_g}. \tag{26}$$

We are only interested in the form of W_C within Γ_{++}.

By examining the behavior of the curves W_G and W_C with respect to $\bar{Q}$, it is straightforward to determine that there exist values $\bar{Q}_1$ and $\bar{Q}_2$ such that, for $\bar{Q} \in (\bar{Q}_1, \bar{Q}_2)$, W_G and W_C cross at two critical points $c_1 = (w_{c1}, y_{c1})$ and $c_2 = (w_{c2}, y_{c2})$ in Γ_{++}. At each of the values $\bar{Q} = \bar{Q}_1$ and $\bar{Q} = \bar{Q}_2$, W_G and W_C touch tangentially at a single critical point. And for $\bar{Q} < \bar{Q}_1$ or $\bar{Q}_2 < \bar{Q}$ there are no critical points. A sketch of this behavior is given in Fig. 5. Critical points c_1 and c_2 are also shown in Fig. 3, which is drawn for the case $\bar{Q}_1 < \bar{Q} < \bar{Q}_2$.

Critical point classification. A critical point is classified by analyzing the solution of the linearized form of (18′) in the local neighborhood of equilibrium[16,20]. With $u = w - w_c$, $v = y - y_c$ denoting the components of a small perturbation from the critical point, the linearized system is

$$\begin{aligned}\begin{pmatrix}\frac{du}{dt}\\ \frac{dv}{dt}\end{pmatrix} &= \begin{pmatrix}\frac{dF}{dw} & \frac{dF}{dy}\\ \frac{dG}{dw} & \frac{dG}{dy}\end{pmatrix}_{w_c,y_c}\begin{pmatrix}u\\ v\end{pmatrix}\\ &= \begin{pmatrix}\frac{F_2}{F_1}\frac{\partial \Delta_H}{\partial w} + \frac{1}{F_1}\frac{\partial \Delta_C}{\partial w} & \frac{F_2}{F_1}\frac{\partial \Delta_H}{\partial y} + \frac{1}{F_1}\frac{\partial \Delta_C}{\partial y}\\ -\frac{\partial \Delta_H}{\partial w} & -\frac{\partial \Delta_H}{\partial y}\end{pmatrix}_{w_c,y_c}\begin{pmatrix}u\\ v\end{pmatrix}.\end{aligned} \tag{27}$$

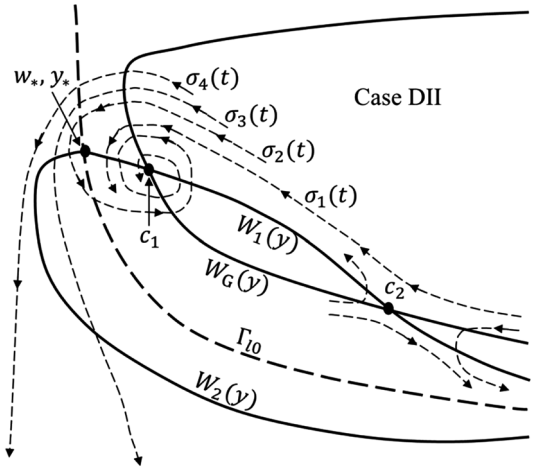

Figure 6. Illustration of possible trajectory behaviors in the vicinity of (w_*, y_*) when the critical point c_1 is a spiral point and c_2 is a saddle. There are four trajectory behaviors, $\sigma_k(t)$, $k = 1, \ldots, 4$, illustrated for $W_2(y)$ having the form in case DII.

In (27) we have used (18′) and the fact that $\Delta_H(w_c, y_c) = \Delta_C(w_c, y_c) = 0$. The matrix in (27) has characteristic values $\Lambda_\pm = (A \pm \sqrt{A^2 - 4D})/2$ where A and D are, respectively, the trace and determinant of the matrix in (27). Characterization of the critical points in terms of A and D is well known[16,20].

Solution trajectories. *Single-phase flow trajectory.* In the single-phase flow regime, the dynamical system variable y satisfies $y(t) = 0$. From (13) we have the relation $w = \overline{K}_C\overline{C}_{Cl}/(1 + \overline{C}_{Cl})$. We use this relation to extend the definition of the variable w into the single-phase regime. Then (2) provides the time development of $w(t)$ during single phase flow.

Transition to two-phase flow; initial condition for gas bubble formation. An initial condition (w_0, y_0) is needed to solve the two-phase flow system (18′). This is set by the initial size of the gas bubble, y_0, and its initial CO_2 concentration, w_0. Initial bubble size is determined by microscopic, non-linear dynamics at a nucleation site[9] that are beyond the scope of this paper. In order to perform numerical computation using a transition from the single-phase to the two-phase region we determine initial bubble formation time, size and CO_2 concentration using approximations outlined in Appendix F. We recognize that conditions (F.1)–(F.3) provide an approximation to actual bubble formation. While we use these conditions in some of our numerical solutions, we also explore other bubble trajectories under the recognition that our initial conditions may not be sufficiently accurate. We note that unless (w_0, y_0) lies on a trajectory that either starts in, or enters, the region $G(w, y) > 0$, the bubble size will monotonically decrease to 0 (the bubble dissolves).

Solution trajectories in Γ_{++} and Γ_{-+}. The sign of the direction field $F(w, y)$ changes across the curves $W_1(y)$, $W_2(y)$, $W_3(y)$; the sign of $G(w, y)$ changes across the curve $W_G(y)$. The critical points c_1 and c_2 play a decisive role in trajectory behaviors. In our numerical computations we show that, as $\overline{Q}$ increases, c_1 changes type: from an unstable node, to an unstable spiral point and then to a stable spiral point; while c_2 always remains a saddle point.

For purposes of illustration of solution trajectories we consider the case when c_1 is a stable spiral point and c_2 is a saddle point. Let $\sigma(t) = (w(t), y(t))$, $w(0) = w_0$, $y(0) = y_0$, be the trajectory of a solution of (18′), where the initial condition $w(0)$, $y(0)$ is assumed to lie in the region Γ_{++}. There are four general patterns for the behavior of $\sigma(t)$. These are illustrated in Fig. 6 which is drawn for $W_2(y)$ having the form of case DII in Appendix D. The first behavior, illustrated by the trajectory labeled $\sigma_1(t)$, is that the trajectory remains in the region of Γ_{++} and spirals into the critical point c_1. The remaining patterns shown involve those trajectories that cross the curve Γ_{l0}. The second trajectory type, $\sigma_2(t)$, does not escape the zone of attraction of the spiral point; it enters the region F^+G^- in Γ_{-+}, re-enters Γ_{++}, and spirals into the critical point c_1. The third, $\sigma_3(t)$, is outside of the zone of attraction; after it enters the region F^+G^- in Γ_{-+}, it never leaves Γ_{-+}, ultimately entering the region F^-G^- and subsequently reaches the w-axis. The last behavior, illustrated by $\sigma_4(t)$, enters and remains in the region F^-G^- after crossing Γ_{l0}; subsequently reaching the w-axis.

For trajectories $\sigma_1(t)$ and $\sigma_2(t)$, the gas bubble in the pore approaches a steady-state size. For trajectories $\sigma_3(t)$ and $\sigma_4(t)$ the bubble first grows to a maximum size before decreasing and ultimately dissolving completely. (See the section below that discusses how trajectories approach the w-axis.)

Solution trajectories Γ_{--}. From the signs of the direction fields on each side of $W_3(y)$ (Fig. 7) we deduce the following behaviors. No trajectory in the F^-G^- region to the right of $W_3(y)$ can enter the F^+G^- region to the left of $W_3(y)$, and any trajectory that starts in the F^+G^- region must exit. In particular, the trajectory labelled $\sigma_d(t)$

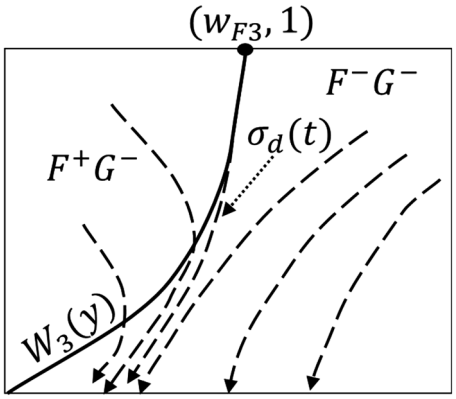

Figure 7. Sketch of solution trajectories in Γ_{--}. All solution trajectories must exit the F^+G^- region. The solution trajectory $\sigma_d(t)$ separates F^+G^- trajectories from all remaining trajectories in the F^-G^- region.

R_{pore}	5×10^{-3} cm	V	5.236×10^{-7} cm^3
a	10^{-3} cm	L	5×10^{-3} cm
T	323.15 K	R	8.31441×10^7 dyne cm mol^{-1}K^{-1}
ν_l	5.4648×10^{-3} dyne s cm^{-2}	ν_g	1.6132×10^{-4} dyne s cm^{-2}
Λ_l	1.4372×10^{-8} cm^{5}dyne^{-1}s^{-1}	Λ_g	4.86854×10^{-6} cm^5 dyne^{-1} s^{-1}
K_C	2.2623×10^7 dyne cm^{-2}	K_H	4.1339×10^4 dyne cm^{-2}
γ	99.0640 dyne cm^{-1}	s	3.96256×10^4 dyne cm^{-2}
p	10^7 dyne cm^{-2}	C_c	4.8×10^{-2} mol

Table 1. Parameters and values used in the numerical computations.

in Fig. 7 that passes through the point $(w_{F3}, 1)$ acts as a separator between trajectories leaving the region F^+G^- and those remaining in the region F^-G^-.

Solution trajectories approaching the ***w****-axis.* Finally, we address the slope of trajectories approaching the $w-$axis. From (18′) and (22) it is straightforward to show that, in the regions Γ_{--} and Γ_{-+},

$$\lim_{y\to 0} \frac{G(w,y)}{F(w,y)} = \frac{\overline{K}_C}{w(1-\overline{K}_C+w)(\overline{K}_C-w)}.$$

Thus the slope, dy/dw, of a trajectory approaches a finite, w-dependent value as $y \to 0$. Consequently, solution trajectories like $\sigma_3(t)$ and $\sigma_4(t)$ in Fig. 6 will evolve toward the w-axis. For such a trajectory, $\sigma(t) = (w(t), y(t))$, there will therefore be a time, t_d, such that $y(t_d) = 0$ (i.e. the bubble is completely dissolved) and $w(t_d)$ is undersaturated. Since $\overline{C}_{Cg}(\overline{C}_C)$ is greater than $w(t_d)$, $w(t)$ will then increase (under single-phase flow conditions) for $t > t_d$ until $w(t)$ reaches a critical saturation value (Appendix F of the supplementary material), a new bubble will form, and a new trajectory cycle will commence.

Numerical computations

Using Maple, numerical computations were performed to verify and illustrate our analytic results. The numerical values of all pore, physical and fluid parameters used in the computations are summarized in Table 1. With these parameter values, (24) sets a flow range limit of $\overline{Q}_{lo} = 7.19379 \times 10^{-5} \le \overline{Q} \le \overline{Q}_{hi} = 3.41059 \times 10^3$. However, the discussion in the section on critical point existence states that critical points can only exist for flows between $\overline{Q}_1$ and $\overline{Q}_2$ (where $\overline{Q}_2 = \overline{Q}_{max}$). From the data in Table 1, we have $\overline{Q}_1 = 1.6 \times 10^{-3}$ and $\overline{Q}_2 = 9.61673 \times 10^3$. Therefore we have the relative sizes $\overline{Q}_{lo} < \overline{Q}_1 < \overline{Q}_{hi} < \overline{Q}_2 = \overline{Q}_{max}$. Note that two critical points always exist for the flow range $\overline{Q}_1 < \overline{Q}_{hi}$ (see Fig. 5b). We perform our numerical computations in this range.

Critical point changes and flow regimes. We first examine the $\overline{Q}$ dependence of the character of the critical point using the linearized model (27). We find three flow regimes: R1: $\overline{Q}_1 \le \overline{Q} < 14.6431$; R2: $14.6431 \le \overline{Q} < 70.7865$ and R3: $70.7865 \le \overline{Q} \le \overline{Q}_{hi}$. In R1 the critical point c_1 is an unstable node; in R2 it is an unstable spiral; and in R3 it is a stable spiral. In all regimes c_2 is a saddle point. Figure 8 shows the movement of the point w_*, y_* and the critical points c_1 and c_2 as a function of $\overline{Q}$. We make the following observations.

(O1) The huge difference in scales between the w- and y-axes distorts perception of angles. Fig. G (supplementary material) shows a properly scaled view of angles in the vicinity of c_2 for $\overline{Q} = 494$.

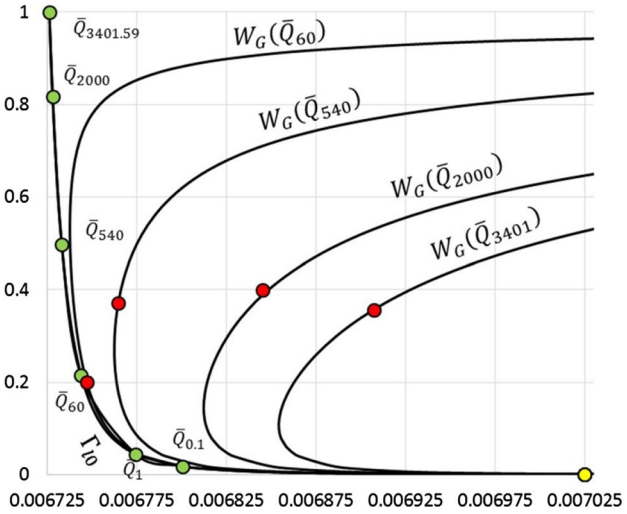

Figure 8. Movement of the points w_*, y_* (green), c_1 (red), and c_2 (yellow) with $\overline{Q}$. The flow rate $\overline{Q}_{\text{value}}$ labels the point w_*, y_* as it moves on the Γ_{l0} curve. The critical points c_1 and c_2 are shown on their respective W_G curves, which are also labeled by the appropriate flow rate.

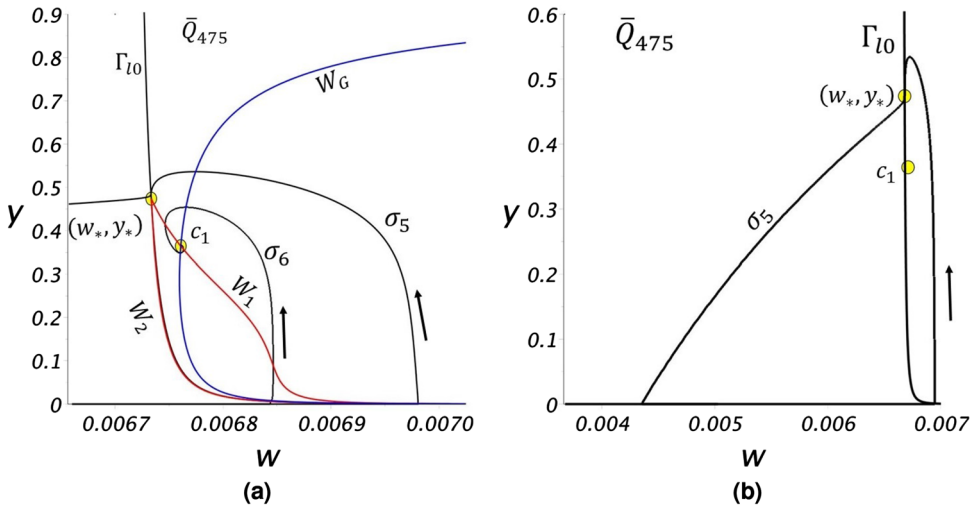

Figure 9. (**a**) A view of two solution trajectories for $\overline{Q} = 475$. For trajectory σ_5, $(w_0, y_0) = (6.9806 \times 10^{-3}, 8 \times 10^{-3})$ and for trajectory σ_6, $(w_0, y_0) = (6.8437 \times 10^{-3}, 8 \times 10^{-3})$. (**b**) A view showing one complete cycle of σ_5.

(O2) The curve W_G closely approaches Γ_{l0}, both in the vicinity of c_2 and as $\overline{Q}$ decreases. This is evident in Fig. 8 and Fig. G (Appendix G).

(O3) The critical point c_2 moves very slowly with $\overline{Q}$, remaining in the close vicinity of the point $(\overline{C}_{\text{Cg}}(\overline{C}_{\text{C}}), y_{l0}(\overline{C}_{\text{C}}))$ with $w_{c2} \leq \overline{C}_{\text{Cg}}(\overline{C}_{\text{C}})$, $y_{c2} > y_{l0}(\overline{C}_{\text{C}})$. At the value $\overline{Q} = \overline{Q}_{\max}$, the critical points c_1 and c_2 coalesce on the $w = \overline{C}_{\text{Cg}}(\overline{C}_{\text{C}})$ boundary.

Gas bubble dynamics. To detail the evolution of gas bubbles, we performed computations using the non-linear system (18′) for a value of $\overline{Q}$ from each regime. The first computation is for regime R3 using the value $\overline{Q} = 475$.

Figure 9a shows a portion of a phase-space trajectory (σ_5). For this value of $\overline{Q}$, using the bubble-point equations (F.1)–(F.3) the pore reaches critical saturation at $t = 8.3296 \times 10^{-3}$. A gas bubble forms in Γ_{++} with $(w_0, y_0) = (6.9806 \times 10^{-3}, 8 \times 10^{-3})$. The gas bubble growth trajectory crosses Γ_{l0} at a time $t_1 = 8.6718 \times 10^{-3}$ at the point $(w_{l0}, y_{l0}) = (6.733216 \times 10^{-3}, 0.484318)$ where $y_{l0} \geq y_*$. At this point, $dw/dt < 0$ and $dy/dt < 0$, σ_5 enters Γ_{-+}, and evolves (Fig. 9b) to the y-axis with the complete dissolution of the bubble at a finite time $t_2 = 8.7116 \times 10^{-3}$. For $t > t_2$, σ_5 follows the w-axis under single-phase flow conditions with $w(t)$ increasing

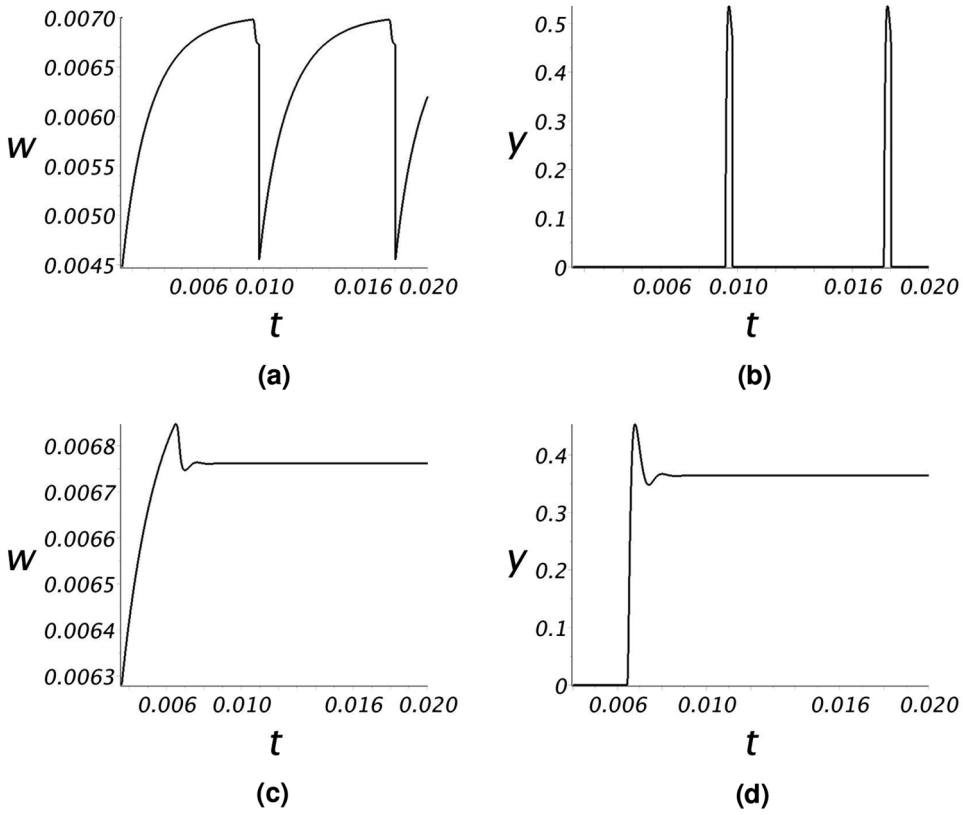

Figure 10. Graphs of (**a**) $w(t)$ and (**b**) $y(t)$ for two cycles of σ_5, and of (**c**) $w(t)$ and (**d**) $y(t)$ for σ_6 of Fig. 9.

until, again using (F.1)–(F.3), at $t_3 = 1.6626 \times 10^{-2}$ the trajectory reaches the bubble point $(6.9806 \times 10^{-3}, 0)$, the gas bubble re-emerges and a new cycle begins. Fig. 9b shows the complete trajectory cycle for σ_5.

Figure 10a,b plot $w(t)$ and $y(t)$ over two cycles of σ_5. The dissolved CO_2 concentration in the liquid phase, $w(t)$, accumulates in the pore until the bubble point is reached. Once the bubble point is reached, time scales shorten dramatically as the bubble expands and subsequently dissolves very rapidly (Fig. 10b). Over this period, the CO_2 concentration in the liquid phase drops precipitously.

Figure 9a also shows the trajectory σ_6 for a bubble that is assumed (i.e. not using equations (F.1)–(F.3)) to form with $(w_0, y_0) = (6.8437 \times 10^{-3}, 8 \times 10^{-3})$. In this case the trajectory lies within the attractor region of c_1 and spirals into the critical point. The values $w(t)$ and $y(t)$ for σ_6 are plotted in Fig. 10c,d, documenting how the dissolved CO_2 concentration in the liquid phase and the gas phase saturation approach steady state values. Note there is a rather sharp oscillation of the bubble prior to reaching steady state.

The second computations explore regime R2 using the flow rate $\overline{Q} = 68$. Only cyclic bubble formation occurs in this flow regime. If a bubble forms sufficiently close to the unstable spiral point, c_1, the cycle may involve an initial period of instability in the bubble growth (Fig. 11a). If the bubble initializes on a more "remote" trajectory, the cycle of bubble formation and dissolution is more regular (Fig. 11b). Fig. 11c,d plot $w(t)$ and $y(t)$ over a time range covering two cycles of the trajectory σ_7 in Fig. 11a.

The third computations explored regime R1 using the flow rate $\overline{Q} = 13$. Only cyclic bubble formation occurs in this flow regime. Trajectories are similar to that shown for σ_8 in Fig. 11b.

Discussion

The mathematical analysis presented in this paper, motivated and supported by our earlier network flow computations[6], leads us to a somewhat unexpected conclusion: namely that when a gas component "bubbles-out" from a saturated solution under steady state flow in porous media, the phase space conditions under which such bubbles achieve a stable size is limited. Our results indicate that, for sufficiently low flow rates (regimes R1 and R2), any gas bubble that forms will re-dissolve, possibly (regime R2) after undergoing oscillatory behavior. In the (much wider) range of faster flow rates (regime R3), whether a gas bubble remains stable or decays depends on the fine-scale details of bubble initiation. In all cases involving bubble dissolution, under steady flow conditions the behavior of bubble formation and re-dissolution repeats cyclically.

Our numerical computations show that these regimes cover a range of conditions pertinent to reservoir flow. Therefore, with respect to flow management in reservoir operations (specifically trying to maintain multi-component, saturated, single phase flow), our results imply that, once pressure conditions allow bubble formation, there is a small "window of opportunity" at low flow rates (regimes R1 and R2) to restrict bubble formation to at

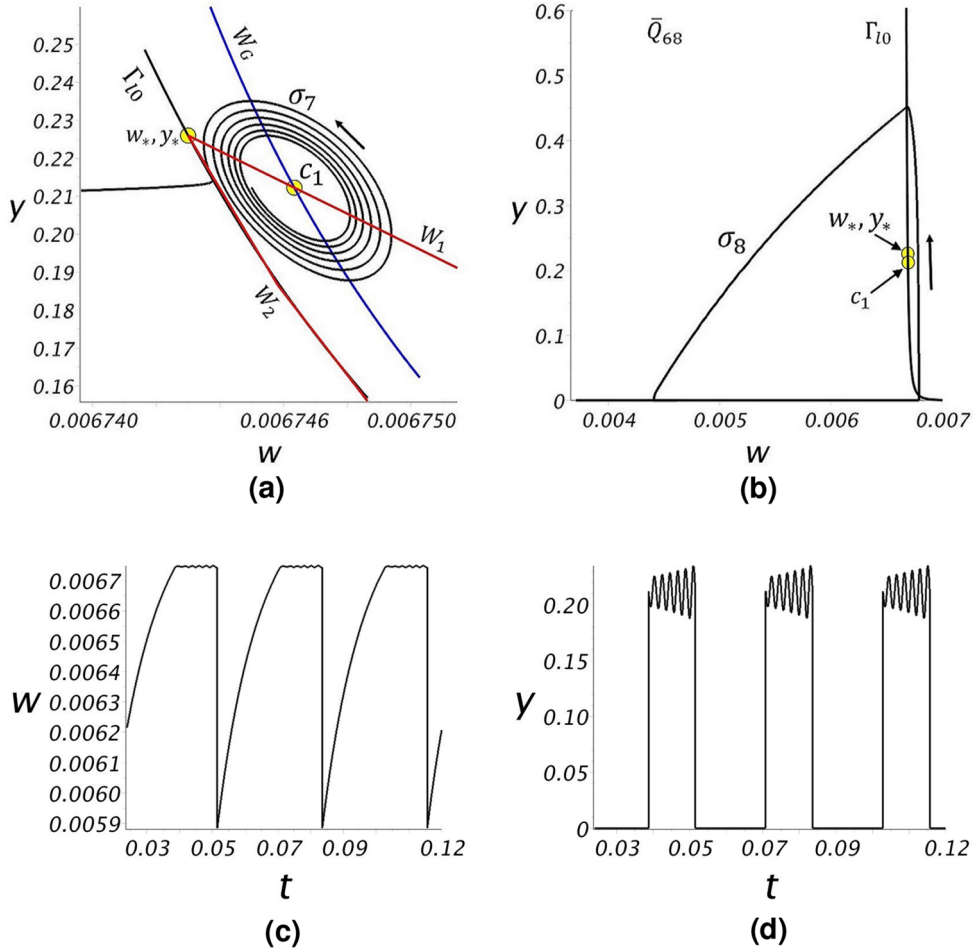

Figure 11. Solution trajectories for $\overline{Q} = 68$ when (**a**) $(w_0, y_0) = (6.744 \times 10^{-3}, 2.12 \times 10^{-1})$ and (**b**) $(w_0, y_0) = (6.83 \times 10^{-3}, 8 \times 10^{-3})$. Graphs of (**c**) w(t) and (**d**) y(t) for three cycles of σ_7.

most cyclic behavior. However once flow rates exceed the rather low threshold delineating regime R3, whether bubbles form stably or cyclically depends on microscopic processes beyond reservoir management control.

Our investigation is not exhaustive; we have analyzed the dynamical system (18′) by employing a number of assumptions. These assumptions are summarized in Appendix H (supplementary material) and fall into two general categories, physical (e.g. liquid phase is perfectly wetting) and technical. The technical assumptions rely on having parameter values similar to petroleum reservoirs (Table 1). We have not investigated removing these assumptions, except to make a comment regarding the flow-rate restriction (24). Two of the inequalities in (24) ensure that the point (w_*, y_*) on Γ_{l0} lies within the phase space. This restriction can be lifted to some extent, allowing (w_*, y_*) to move somewhat outside of the phase space. Reducing this restriction will extend the analysis to a larger range of flow values but will produce little change in the qualitative aspects of our analysis.

The y-dependence in the dynamical system is a critical determinant in the resulting behavior. This dependence comes from three sources: the capillary pressure term (10) where we assume $r = y^{1/3}\mathrm{R}_{\mathrm{pore}}$, the distribution of water and CO_2 mass (16) where the y-dependence is linear, and from the fractional flow functions $f(y)$ and $g(y)$ which introduce complicated nonlinear dependence. It is possible that different forms for the fractional flow functions could significantly alter the gas bubble behavior of this dynamical system.

One possible critique of our analysis is that bubble dissolution, which is governed by the evolution of trajectories in Γ_{--} and Γ_{-+} (i.e. under back-flow conditions), is solely due to our assumption that back-flow involves pure water invading the pore from the outlet reservoir. Such back-flow reduces $\overline{C}_{\mathrm{Cl}}$ concentration in the pore, potentially forcing dissolution of the gas phase. In actual porous media flow situations, back-flow would involve water containing CO_2 (at concentrations less than $\overline{C}_{\mathrm{Cl}}$) infiltrating the pore. Back-flow under these more realistic conditions would affect the shape of trajectories in the regions Γ_{--} and Γ_{-+}, opening the possibility that trajectories that enter Γ_{-+} from Γ_{++} may re-enter Γ_{++}. However, changing back-flow conditions should not affect the analysis in Γ_{++}, and specifically not affect the type of critical points. Thus, at low flow conditions there would still be no attractor node to produce stable bubbles. At higher flow rates a stable spiral node exists, but it has a finite-sized region of attraction (as can be inferred from trajectory segments in the vicinity of the saddle c_2 in Fig. 6). Thus not all trajectories would lead to the growth of stable bubbles. Finally, we note that our computations in Chang and Lindquist[6], which included realistic back-flow conditions, did produce bubble dissolution.

While we have examined the case where the gas phase is CO_2, the analysis should hold for any other gas that preserves the assumptions used. Similarly, we have considered a liquid phase consisting solely of H_2O, with dissolved CO_2. This invites the question of how applicable our analysis is to a more complicated brine phase.

Received: 9 October 2019; Accepted: 2 July 2020
Published online: 06 August 2020

References

1. Abadpour, A. & Panfilov, M. Method of negative saturations for modeling two-phase compositional flow with oversaturated zones. *Transp. Porous Med.* **79**, 197–214 (2009).
2. Amaziane, B., Jurak, M. & Keko, A. Z. Modeling compositional compressible two-phase flow in porous media by the concept of the global pressure. *Comput. Geosci.* **18**, 297–309 (2014).
3. Belhaj, H., Abukhalifeh, H. & Javid, K. Miscible oil recovery utilizing N_2 and/or HC gases in CO_2 injection. *J. Pet. Sci. Eng.* **111**, 144–152 (2013).
4. Bourgeat, A., Jurak, M. & Smai, F. Two-phase, partially miscible flow and transport modeling in porous media: application to gas migration in a nuclear waste repository. *Comput. Geosci.* **13**, 29–42 (2009).
5. Bourgeat, A., Jurak, M. & Smai, F. On persistent primary variables for numerical modeling of gas migration in a nuclear waste repository. *Comput. Geosci.* **17**, 287–305 (2013).
6. Chang, K. A. & Lindquist, W. B. A network flow model for the genesis and migration of gas phase. *Comput. Geosci.* **17**, 67–81 (2013).
7. Chen, Z. & Ewing, R. E. From single-phase to compositional flow: applicability of mixed finite elements. *Transp. Porous Med.* **27**, 225–242 (1997).
8. Class, H., Helmig, R. & Bastian, P. Numerical simulation of non-isothermal multiphase multicomponent processes in porous media. *Adv. Water Resour.* **25**, 533–550 (2002).
9. Epstein, P. S. & Plesset, M. S. On the stability of gas bubbles in liquid–gas solutions. *J. Chem. Phys.* **18**, 1505–1509 (1950).
10. Ern, A. & Mozolevski, I. Discontinuous Galerkin method for two-component liquid–gas porous media flows. *Comput. Geosci.* **16**, 677–690 (2012).
11. Fourar, M. & Lenormand, R. *A viscous coupling model for relative permeabilities in fractures*, SPE 49006, SPE Annual Technical Conference and Exhibition, New Orleans, LA, USA (1998).
12. Gale, J. & Davison, J. Transmission of CO_2-safety and economic considerations. *Energy* **29**, 1319–1328 (2004).
13. Ho, C. K. & Webb, S. W. (eds) *Gas Transport in Porous Media* (Springer, Dordrecht, 2006).
14. Hussen, C., Amin, R., Madden, G. & Evans, B. Reservoir simulation for enhanced gas recovery: an economic evaluation. *J. Nat. Gas Sci. Eng.* **5**, 42–50 (2012).
15. Jaffre, J. & Sboui, A. Henrys law and gas phase disappearance. *Transp. Porous Media* **82**, 521–526 (2010).
16. Khalil, H. K. *Nonlinear Systems* 3rd edn, 111–182 (Prentice-Hall, Upper Saddle River, 2002).
17. Kulkarni, A. A. & Joshi, J. B. Bubble formation and bubble rise velocity in gas–liquid systems: a review. *Ind. Eng. Chem. Res.* **44**, 5873–5931 (2005).
18. Lide, D. R. & Kehiaian, H. V. *CRC Handbook of Thermophysical and Thermochemical Data* 405–412 (CRC Press, New York, 1994).
19. McCoy, S. T. & Rubin, E. S. An engineering-economic model of pipeline transport of CO_2 with application to carbon capture and storage. *Int. J. Greenh. Gas Control* **2**, 219–229 (2008).
20. Nagle, R. K., Saff, E. B. & Snider, A. D. *Fundamentals of Differential Equations and Boundary Value Problems* 6th edn, 718–782 (Pearson Education Limited, London, 2012).
21. Neumann, R., Bastian, P. & Ippisch, O. Modeling and simulation of two-phase two-component flow with disappearing nonwetting phase. *Comput. Geosci.* **17**, 139–149 (2013).
22. Oldenburg, C. M. Carbon dioxide as cushion gas for natural gas storage. *Energy Fuels* **17**, 240–246 (2008).
23. Robin, R., Behot, J. & Sygouni, V. *CO_2 injection in porous media: observations in glass micromodels under reservoir conditions*, SPE paper 154165-PP, Eighteenth SPE Improved Oil Recovery Symposium, Tulsa, OK, 14–18 (2012).
24. Thomas, S. Enhanced oil recovery—an overview. *Oil Gas Sci. Technol.* **63**, 9–19 (2008).
25. Vandeginste, V. & Piessens, K. Pipeline design for a least-cost router application for CO_2 transport in the CO_2 sequestration cycle. *Int. J. Greenh. Gas Control* **2**, 571–581 (2008).
26. Wardlaw, N. C. The effects of geometry, wettability, viscosity and interfacial-tension on trapping in single pore throat pairs. *J. Can. Pet. Technol.* **21**, 21–27 (1982).
27. Wheeler, M. F., Delshad, M., Kong, X., Thomas, S., Wildey, T. & Xue, G. Role of computational science in protecting the environment: geological storage of CO_2, in *Proceeding of the International Congress of Mathematicians, Hyderabad, India*, 2864–2885 (2010).
28. Zhang, Z. X., Wang, G. X., Massarotto, P. & Rudolph, V. Optimization of pipeline transport for CO_2 sequestration. *Energy Convers. Manag.* **47**, 702–715 (2006).

Acknowledgements

This research was supported partially by the Ministry of Science and Technology of the Republic of China under Grant 106-2115-M153-001.

Author contributions

K.A.C. performed the numerical computations. K.A.C. and W.B.L. contributed to the mathematical analysis and writing the manuscript.

Competing interests

The authors declare no competing interests.

Additional information

Supplementary information is available for this paper at https://doi.org/10.1038/s41598-020-69506-w.

Correspondence and requests for materials should be addressed to K.A.C.

Reprints and permissions information is available at www.nature.com/reprints.

Supplement: The Dynamics of Gas-Bubble Formation at Saturated Conditions in Porous Media Flow

K. Alex Chang[1,*] **and W. Brent Lindquist**[2]

[1]National Pingtung University, Department of Applied Mathematics, Pingtung, Taiwan, ROC.
[2]Texas Tech University, Departments of Mathematics & Statistics and Geosciences, Lubbock Texas, USA.
[*]chang@mail.nptu.edu.tw

Appendix A The direction field $dy/dt = G(w,y)$

From (18′), (15′a), (7′a), and (14′) we start with the expression for the direction field $dy/dt = G(w,y)$,

$$G(w,y) = -\overline{Q} + \overline{\Lambda}_l f(y)[w - \overline{p} - \bar{s}y^{-1/3}], \tag{A.1}$$

where $f(y)$ is given by (8). It will simplify exposition (just for this appendix) to switch variables from (w,y) to (ω,z) defined by $\omega = [w-\overline{p}]/\bar{s}$, $z = y^{1/3}$. The map $\omega(w)$ has the range $\omega \in [-\overline{p}/\bar{s}, \omega(\overline{C}_C)]$ where $\omega(\overline{C}_C) \stackrel{\text{def}}{=} [\overline{C}_{Cg}(\overline{C}_C) - \overline{p})]/\bar{s}$. The points $w = \overline{p}$ and $w = \overline{p} + \bar{s}$ correspond to the values $\omega = 0$ and $\omega = 1$ respectively. Under this change of variables, (A.1) can be written

$$\frac{G(\omega,z)}{\overline{\Lambda}_l \bar{s}} = -\frac{\overline{Q}}{\overline{\Lambda}_l \bar{s}} + f(z)[\omega - z^{-1}]. \tag{A.2}$$

We consider the isoclines of $G(\omega,z)$. Parametrizing the isoclines by the value $G = \beta\overline{Q}$, where β is a free parameter, from (A.2) each isocline has the form

$$\omega(z;\alpha) = \frac{1}{z} + \frac{\alpha}{f(z)}, \qquad \text{where} \quad \alpha = (1+\beta)\overline{Q}/(\overline{\Lambda}_l \bar{s}). \tag{A.3}$$

The value $\alpha = 0$ (i.e. $\beta = -1$) corresponds to the curve Γ_{l0} on which $G = -\overline{Q}$. The equation for Γ_{l0} in (ω,z) space is $\omega(z,0) = 1/z$. The $\alpha > 0$ isoclines correspond to $\overline{Q}_l > 0$, thus they cover the region Γ_{++}, while the $\alpha < 0$ isoclines cover the regions Γ_{-+} and Γ_{--}. From (A.3) note that all isoclines have the value $G < 0$ in Γ_{-+} and Γ_{--}. Thus the condition $G = 0$ is only possible in the region Γ_{++}.

We first consider the $\alpha > 0$ isoclines. From (8), in Γ_{++} $f(z)$ has the form, $f(z) = (1+z^3/2)(1-z^3)^2$. It is straightforward to show that $f(z)$ is monotonically decreasing on $z \in [0,1]$ with $f(0) = 1$, $f(1) = 0$, $f'(0) = f'(1) = 0$, $f'(z) < 0$, and $f''(z) < 0$ on $(0, 2^{-1/3})$ while $f''(z) > 0$ on $(2^{-1/3}, 1]$. Defining $h(z) = 1/f(z)$, we have

$$\omega(z;\alpha) = 1/z + \alpha h(z) > \omega(z;0), \tag{A.4}$$

which satisfies $d^2\omega(z;\alpha)/dz^2 > 0$. For $\alpha > 0$, $\omega(z;\alpha)$ is a function that is "concave up" having a unique minimum $\omega_{\min}(\alpha)$ at the point $z_{\min}(\alpha) \in (0,1)$ satisfying,

$$z_{\min}^2 h'(z_{\min}) = \alpha^{-1}, \qquad \omega_{\min}(\alpha) = 1/z_{\min} + \alpha h(z_{\min}). \tag{A.5}$$

In physical space ω is bounded above by the value $\omega(\overline{C}_C)$. However, viewed as a function of z, (A.3) implicitly extends the range of ω values comprising the α'th islocline to $\omega(z;\alpha) \in [\omega_{\min}(\alpha), \infty]$ with $\lim_{z\to 0^+} \omega(z;\alpha) = \lim_{z\to 1^-} \omega(z;\alpha) \to \infty$. There exists some isocline value $\alpha_{\max} > 0$ such that $\omega_{\min}(\alpha_{\max}) = \omega(\overline{C}_C)$ and $\omega_{\min}(\alpha) < \omega(\overline{C}_C)$ for $0 < \alpha < \alpha_{\max}$. Consequently, from (A.4) and (A.5) we conclude there exist values $z_{G1}(\alpha)$ and $z_{G2}(\alpha)$ satisfying $0 < z_{G1}(\alpha) < z_{\min}(\alpha) < z_{G2}(\alpha) < 1$ such that

$$\omega(z_{G1}(\alpha);\alpha) = \omega(z_{G2}(\alpha);\alpha) = \omega(\overline{C}_C) \quad \text{for} \quad \alpha < \alpha_{\max}.$$

For the isocline $\omega(z;\alpha_{\max})$, we have $z_{G1}(\alpha_{\max}) = z_{\min}(\alpha_{\max}) = z_{G2}(\alpha_{\max})$. Fig. A.1(a) provides a sketch of the isoclines $\omega(z;0)$ and $\omega(z;\alpha < \alpha_{\max})$, indicating the points $(\omega_{\min}(\alpha), z_{\min}(\alpha))$, $(\omega(\overline{C}_C), z_{G1}(\alpha))$ and $(\omega(\overline{C}_C), z_{G2}(\alpha))$.

The value of $\alpha_{\max}$ places restrictions on $\overline{Q}$. From (A.3) we note that the isocline $\alpha = \overline{Q}/(\overline{\Lambda}_l \bar{s})$ carries the constant value $G = 0$. Therefore if $\overline{Q}/(\overline{\Lambda}_l \bar{s}) > \alpha_{\max}$, then $G < 0$ everywhere in Γ_{++} (and therefore everywhere in the physical phase space).

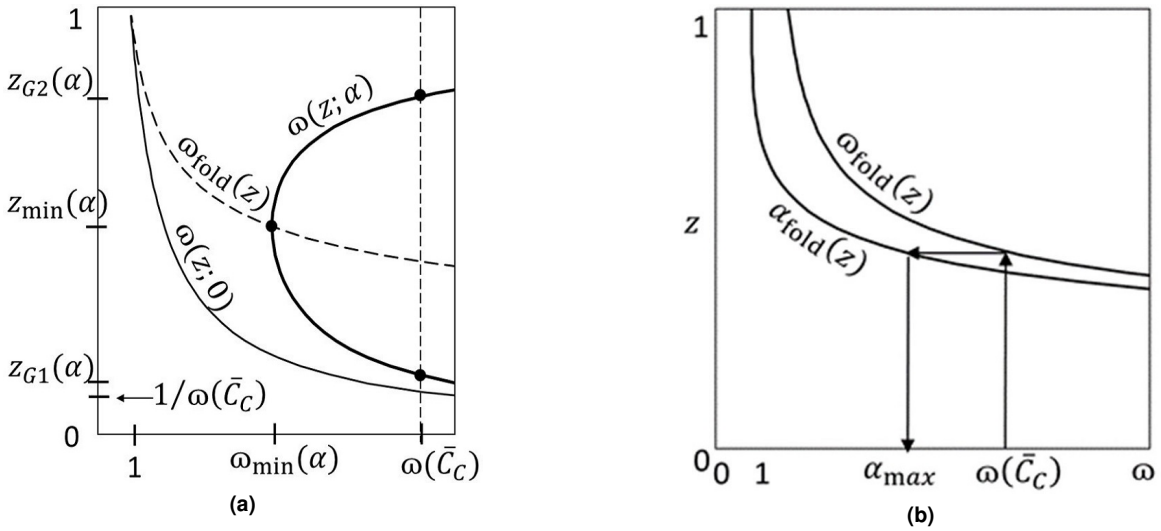

Figure A.1. (a) Plots of $\Gamma_{l0} = \omega(z;0)$ and example isocline $\omega(z;\alpha)(\alpha < \alpha_{\max})$ showing the fold curve $\omega_{\text{fold}}(z)$ and the values $z_{G1}(\alpha)$, $z_{\min}(\alpha)$, $z_{G2}(\alpha)$, $\omega_{\min}(\alpha)$, and $\omega(\bar{C}_C)$. (b) Plots of the curves (A.7a) and (A.8) and an illustration of the computation needed to determine the value $\alpha_{\max}$.

Consequently, the direction field dy/dt would be negative everywhere in the physical phase space and no critical point could exist. Under these conditions, any gas bubble that tries to form dissolves rapidly and the physical phase space will not support gas bubbles. Therefore $\overline{Q}$ must be sufficiently small such that

$$\overline{Q} < \alpha_{\max}\overline{\Lambda}_l \bar{s} \stackrel{\text{def}}{=} \overline{Q}_{\max}. \tag{A.6}$$

To compute $\alpha_{\max}$ note that, as α increases from the value 0, the points $(z_{\min}(\alpha), \omega_{\min}(\alpha))$ trace out a curve. This curve defines a "fold" in the function $G(\omega, z)$ across which G achieves maximum values in the z (but not ω) direction. The parameter α can be eliminated from the two equations in (A.5) giving the equation for this fold curve,

$$\omega_{\text{fold}}(z) = \frac{1}{z} + \frac{h(z)}{z^2 h'(z)} = \frac{2}{9}\frac{(1+2z^3)^2}{z^4(1+z^3)}. \tag{A.7a}$$

Note that $\omega_{\text{fold}}(z) > 0$ on $[0,1]$ with $\omega_{\text{fold}}(1) = 1$. In w, y coordinates, the fold curve will be denoted

$$W_{\text{fold}}(y) = \overline{p} + \bar{s}\frac{2}{9}\frac{(1+2y)^2}{y^{4/3}(1+y)}. \tag{A.7b}$$

A sketch of the curve $\omega_{\text{fold}}(z)$ is also provided in Fig. A.1(a).

Inverting the first equation in (A.5) gives the values of α along the fold curve $\omega_{\text{fold}}(z)$,

$$\alpha_{\text{fold}}(z) = \frac{1}{z^2 h'(z)} = \frac{2}{9}\frac{(1+z^3/2)^2(1-z^3)^3}{z^4(1+z^3)}. \tag{A.8}$$

Note that the right-hand sides of (A.7a) and (A.8) are only functions of z (i.e. of $y = s_g$), independent of any other physical parameter in the problem. Thus the two curves $\omega_{\text{fold}}(z)$ and $\alpha_{\text{fold}}(z)$ can be computed, independent of any particular flow problem in this geometry. These two curves are plotted in Fig. A.1(b). This figure illustrates how $\alpha_{\max}$ is computed and how the physical parameters ($\overline{K}_C$, $\overline{C}_C$, $\overline{p}$, $\bar{s}$ and $\overline{\Lambda}_l$) enter through the value $w(\overline{C}_C)$ and the computation (A.6) for $\overline{Q}_{\max}$.

With the value of $\overline{Q}$ restricted by (A.6), the isocline $G(w,y) = 0$ exists in Γ_{++}. In the text we shall refer to this isocline as the curve $W_G(y)$ (see Fig. A.2(a)), and the two values where this curve intersects the boundary $w = \overline{C}_{Cg}(\overline{C}_C)$ will be denoted y_{G1} and y_{G2}, where $y_{G1} < y_{G2}$.

We will have need of the partial derivatives $\partial G(w,y)/\partial w$ and $\partial G(w,y)/\partial y$. In Γ_{++} these can be computed directly from

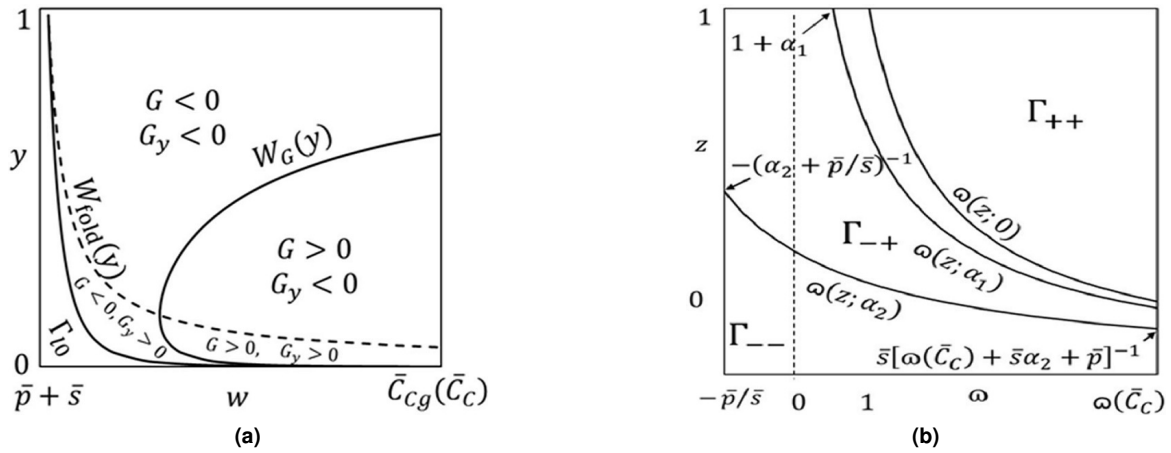

Figure A.2. (a) Variation of the sign of $G(w,y)$ and its partial derivative G_y in Γ_{++}. Note that the curves Γ_{l0} and $W_G(y)$ may approach very close, but do not cross. (b) Example $G(\omega,z)$ isoclines in Γ_{-+} and Γ_{--}, showing axis intersection values.

(A.1):

$$\frac{\partial G(w,y)}{\partial w} = \overline{\Lambda}_l f(y) \begin{cases} >0 & \text{on} \quad y\in[0,1), \\ =0 & \text{for} \quad y=1, \end{cases}$$
$$\frac{\partial G(w,y)}{\partial y} = \overline{\Lambda}_l f'(y)\left\{w-\overline{p}-\overline{s}\left[\frac{1}{y^{1/3}}-\frac{f(y)}{3f'(y)y^{3/4}}\right]\right\} = -\frac{3}{2}\overline{\Lambda}_l(1-y)^2[w-W_{\rm fold}(y)].$$

Note that $\partial G(w,y)/\partial y = 0$ on the curves $y=1$ and $W_{\rm fold}(y)$. Thus when crossing the curve $W_{\rm fold}(y)$, the partial $\partial G(w,y)/\partial y$ changes sign, while the sign of the partial $\partial G(w,y)/\partial w$ remains unchanged. Fig. A.2(a) illustrates the respective signs of $G(w,y)$ and its partial derivative G_y in Γ_{++}.

We now consider the form of the isoclines for $\alpha<0$ in the regions Γ_{-+} and Γ_{--}. With $f(z)=1$, the equation of each isocline is simply

$$\omega(z;\alpha) = \frac{1}{z}+\alpha. \tag{A.9}$$

Fig. A.2(b) plots two of these isoclines showing relevant intersection points with the physical axes. Note that as $\alpha\to-\infty$, the isoclines approach the $z=0$ axis.

The needed partial derivatives of $G(w,y)$ in Γ_{-+} and Γ_{--} are straightforward to compute from (A.1) (with $f(y)=1$),

$$\frac{\partial G(w,y)}{\partial w} = \overline{\Lambda}_l > 0, \qquad \frac{\partial G(w,y)}{\partial y} = \frac{\overline{\Lambda}_l\overline{s}}{3y^{4/3}} > 0.$$

There is no change in the signs of $G(w,y)$ or its partial derivatives G_w, G_y across the curves Γ_{l0} or Γ_{g0}.

Appendix B $\widetilde{F}(w,y)$ on Γ_{l0}

We address the sign of $\widetilde{F}(w,y)$ along the curve Γ_{l0}. We begin with the form of $\widetilde{F}(w,y)$ in (23b) which we write as

$$\widetilde{F}(w,y)|_{\Gamma_{l0}} = \overline{\Lambda}_{\rm g}\overline{s}(\overline{K}_{\rm C}-w)w\left[\frac{\overline{Q}}{\overline{\Lambda}_{\rm g}\overline{s}}\left(1+\frac{\overline{C}_{\rm C}}{w}-\frac{1}{\overline{K}_{\rm C}-w}\right)-\left(\frac{\overline{s}}{w-\overline{p}}\right)^8\right]$$
$$\stackrel{\rm def}{=} H_1(w)\left[H_2(w)-\left(\frac{\overline{s}}{w-\overline{p}}\right)^8\right]. \tag{B.10}$$

Our interest is in the domain $\overline{p}+\overline{s}\le w\le\overline{C}_{\rm Cg}(\overline{C}_{\rm C})$. Here $H_1(w)>0$. From restriction (24) we note that

$$\frac{\overline{Q}}{\overline{\Lambda}_{\rm g}\overline{s}}\left(1+\frac{\overline{C}_{\rm C}}{\overline{p}+\overline{s}}-\frac{1}{\overline{K}_{\rm C}-\overline{p}-\overline{s}}\right)<1, \qquad \frac{\overline{Q}}{\overline{\Lambda}_{\rm g}\overline{s}} > \left(\frac{\overline{s}}{\overline{C}_{\rm Cg}(\overline{C}_{\rm C})-\overline{p}}\right)^8. \tag{B.11}$$

Lemma B. *Given* (B.11) *and the assumption*

$$\frac{4\overline{K}_{\rm C}}{(1+\overline{C}_{\rm C}+\overline{K}_{\rm C})^2} \ll 1, \tag{B.12}$$

then $\widetilde{F}(w,y)|_{\Gamma_{l0}} = 0$ *at a single point* w_*, $y_* = y_{l0}(w_*)$ *where* $\overline{p}+\overline{s} < w_* < \overline{C}_{\rm Cg}(\overline{C}_{\rm C})$.

Proof: We show that the functions $H_2(w)$ and $y_{l0}(w)^{8/3} = [\overline{s}/(w-\overline{p})]^8$ in (B.10) intersect at a single value w_* in the interval $(\overline{p}+\overline{s}, \overline{C}_{\rm Cg}(\overline{C}_{\rm C}))$. We proceed by elucidating the properties of $H_2(w)$ and $y_{l0}(w)^{8/3}$ needed for this proof. For $H_2(w)$ we have the following observations:

$$\begin{array}{ll} \lim\limits_{w\to 0^+} H_2(w) \to \infty; & \lim\limits_{w\to \overline{K}_{\rm C}} H_2(w) \to -\infty; \\ H_2(w_+) = 0, \quad \text{where} & w_+ \approx \overline{C}_{\rm Cg}(\overline{C}_{\rm C}+\overline{K}_{\rm C}) \text{ and } \overline{C}_{\rm Cg}(\overline{C}_{\rm C}) < w_+ < \overline{K}_{\rm C}. \end{array} \tag{B.13}$$

To verify (B.13), note from (B.10) that $H_2(w) = 0$ for w satisfying $w^2 + (\overline{C}_{\rm C}+\overline{K}_{\rm C})w - \overline{C}_{\rm C}\overline{K}_{\rm C} = 0$. Solving this quadratic for the positive root under assumption (B.12) we have, to first order in a Taylor expansion of the square-root of the quadratic discriminant,

$$w_+ \approx \frac{\overline{K}_{\rm C}(\overline{C}_{\rm C}+\overline{K}_{\rm C})}{1+\overline{C}_{\rm C}+\overline{K}_{\rm C}}.$$

The first two derivatives of $H_2(w)$ are

$$H_2'(w) = -\frac{\overline{Q}}{\overline{\Lambda}_{\rm g}\overline{s}}\left[\frac{\overline{C}_{\rm C}}{w^2} + \frac{1}{(\overline{K}_{\rm C}-w)^2}\right] < 0, \qquad H_2''(w) = 2\frac{\overline{Q}}{\overline{\Lambda}_{\rm g}\overline{s}}\left[\frac{\overline{C}_{\rm C}}{w^3} - \frac{1}{(\overline{K}_{\rm C}-w)^3}\right]. \tag{B.14}$$

From (B.14), $H_2''(w)$ must have a single root in the interval $w \in (0, \overline{K}_{\rm C})$. Since $\lim_{w\to 0^+} H_2''(w) > 0$ and

$$\begin{aligned} H_2''(\overline{C}_{\rm Cg}(\overline{C}_{\rm C})) &= 2\frac{\overline{Q}}{\overline{\Lambda}_{\rm g}\overline{s}}\left[\frac{\overline{C}_{\rm C}}{(\overline{C}_{\rm Cg}(\overline{C}_{\rm C}))^3} - \frac{1}{(\overline{K}_{\rm C}-\overline{C}_{\rm Cg}(\overline{C}_{\rm C}))^3}\right] \\ &= 2\frac{\overline{Q}}{\overline{\Lambda}_{\rm g}\overline{s}}\frac{\overline{C}_{\rm C}(1-\overline{C}_{\rm C}^2)}{(\overline{C}_{\rm Cg}(\overline{C}_{\rm C}))^3} > 0, \end{aligned} \tag{B.15}$$

then the single root of $H_2''(w)$ must lie between $\overline{C}_{\rm Cg}(\overline{C}_{\rm C})$ and $\overline{K}_{\rm C}$. In (B.15) we have used the fact that $\overline{C}_{\rm C} < 1$. Thus from (B.14) and (B.15) we have

$$H_2''(w) > 0 \text{ on } (0, \overline{C}_{\rm Cg}(\overline{C}_{\rm C})). \tag{B.16}$$

For $y_{l0}(w)^{8/3}$ we have the observations that, for $w > 0$,

$$\frac{d}{dw}(y_{l0}(w))^{8/3} = -8(y_{l0}(w))^3\,\overline{s}^{-1} < 0, \tag{B.17a}$$

$$\frac{d^2}{dw^2}(y_{l0}(w))^{8/3} = 72(y_{l0}(w))^{10/3}\,\overline{s}^{-2} > 0. \tag{B.17b}$$

Equations (B.14), (B.16) and (B.17) state that $H_2(w)$ and $y_{l0}(w)^{8/3}$ are both monotonic, decreasing, concave-up functions on the interval $(0, \overline{C}_{\rm Cg}(\overline{C}_{\rm C}))$. In addition (B.11) guarantees that $H_2(\overline{p}+\overline{s}) < y_{l0}(\overline{p}+\overline{s})^{8/3}$ and $H_2(\overline{C}_{\rm Cg}(\overline{C}_{\rm C})) > y_{l0}(\overline{C}_{\rm Cg}(\overline{C}_{\rm C}))^{8/3}$. Thus we have the existence of a single value w_* in the interval $(\overline{p}+\overline{s}, \overline{C}_{\rm Cg}(\overline{C}_{\rm C}))$ such that $H_2(w_*) = y_{l0}(w_*)^{8/3}$, i.e. such that $\widetilde{F}(w_*, y_{l0}(w_*)) = 0$. Let $y_* \stackrel{\rm def}{=} y_{l0}(w_*)$. ■

As a consequence of Lemma B, we have

$$\widetilde{F}(w, y_{l0}(w)) \begin{cases} < 0, & w \in [\overline{p}+\overline{s}, w_*), \\ = 0, & w = w_*, \\ > 0, & w \in (w_*, \overline{C}_{\rm Cg}(\overline{C}_{\rm C})]. \end{cases} \tag{B.18}$$

Appendix C $\widetilde{F}(w,y)$ in Γ_{++}

We address the variation of the sign of $\widetilde{F}(w,y)$ in Γ_{++} by analyzing (23a). We begin with the behavior of $\widetilde{F}(w,y)$ on the boundaries of Γ_{++}. The behavior of $\widetilde{F}(w,y)$ on the boundary Γ_{l0} was analyzed in Appendix B. On the boundary $y=1$,

$$\widetilde{F}(w,1)=\overline{\Lambda}_{\rm g}\bar{s}(\overline{K}_{\rm C}-w)(F_2(w)+\overline{C}_{\rm C})\left\{\frac{\overline{Q}}{\overline{\Lambda}_{\rm g}\bar{s}}-\frac{w(w-\overline{p})}{(F_2(w)+\overline{C}_{\rm C})\bar{s}}\right\}. \tag{C.19}$$

On this boundary, $\overline{p}+\bar{s}\le w\le \overline{C}_{\rm Cg}(\overline{C}_{\rm C})<\overline{K}_{\rm C}$; therefore the term $(\overline{K}_{\rm C}-w)(F_2(w)+\overline{C}_{\rm C})$ is positive. In addition,

$$\frac{\overline{Q}}{\overline{\Lambda}_{\rm g}\bar{s}}<\frac{(\overline{p}+\bar{s})}{(F_2(\overline{p}+\bar{s})+\overline{C}_{\rm C})}\frac{(\overline{p}+\bar{s}-\overline{p})}{\bar{s}}<\frac{w(w-\overline{p})}{(F_2(w)+\overline{C}_{\rm C})\bar{s}}, \tag{C.20}$$

where the first inequality in (C.20) comes from (24). By (C.20), $\widetilde{F}(w,1)<0$ for $\overline{p}+\bar{s}\le w\le\overline{C}_{\rm Cg}(\overline{C}_{\rm C})<\overline{K}_{\rm C}$.

The final boundary is $w=\overline{C}_{\rm Cg}(\overline{C}_{\rm C})$, $y\in(y_{l0}(\overline{C}_{\rm C}),1)$. Using (18′) and (15′), we can derive an expression relating $\widetilde{F}(w,y)$ and $G(w,y)$,

$$\widetilde{F}(w,y)=(\overline{K}_{\rm C}-w)\{-[F_2(w)+\overline{C}_{\rm C}]G(w,y)+(\overline{C}_{\rm C}-\overline{C}_{Cl}(w))\overline{Q}_l(w,y)-w\overline{Q}_{\rm g}(w,y)\}.$$

This expression simplifies considerably when evaluated at $w=\overline{C}_{\rm Cg}(\overline{C}_{\rm C})$,

$$\widetilde{F}(\overline{C}_{\rm Cg}(\overline{C}_{\rm C}),y)=-\frac{\overline{K}_{\rm C}^2\overline{C}_{\rm C}}{(1+\overline{C}_{\rm C})^2}\left\{G(\overline{C}_{\rm Cg}(\overline{C}_{\rm C}),y)+\overline{Q}_{\rm g}(\overline{C}_{\rm Cg}(\overline{C}_{\rm C}),y)\right\}. \tag{C.21}$$

We note that $\overline{Q}_{\rm g}(\overline{C}_{\rm Cg}(\overline{C}_{\rm C}),y)>0$. From (C.21) and the results on the signs of $G(w,y)$ summarized in Fig. A.2(a), we have

$$\widetilde{F}(\overline{C}_{\rm Cg}(\overline{C}_{\rm C}),y)<0\quad\text{for}\quad y\in[y_{\rm G1},y_{\rm G2}]. \tag{C.22}$$

From (B.18) we have

$$\widetilde{F}(\overline{C}_{\rm Cg}(\overline{C}_{\rm C}),y_{l0}(\overline{C}_{\rm C}))>0. \tag{C.23}$$

Taking the derivative of (C.21) with respect to y yields

$$\frac{d\widetilde{F}(\overline{C}_{\rm Cg}(\overline{C}_{\rm C}),y)}{dy}=-\frac{\overline{K}_{\rm C}^2\overline{C}_{\rm C}}{(1+\overline{C}_{\rm C})^2}\left\{\frac{dG(\overline{C}_{\rm Cg}(\overline{C}_{\rm C}),y)}{dy}+3\overline{\Lambda}_{\rm g}\left(\overline{C}_{\rm Cg}(\overline{C}_{\rm C})-\overline{p}\right)y^2\right\}. \tag{C.24}$$

From (C.24) and the results on the signs of the partial $\partial G/\partial y$ summarized in Fig. A.2(a), we conclude

$$\frac{d\widetilde{F}(\overline{C}_{\rm Cg}(\overline{C}_{\rm C}),y)}{dy}<0\quad\text{for}\quad y\in[y_{l0}(\overline{C}_{\rm C}),y_{\rm G1}]. \tag{C.25}$$

Therefore (C.22), (C.23) and (C.25) imply there exists a single value $y_{\rm F1}$ such that

$$\widetilde{F}(\overline{C}_{\rm Cg}(\overline{C}_{\rm C}),y_{\rm F1})=0\ \text{ with }\ y_{l0}(\overline{C}_{\rm Cg}(\overline{C}_{\rm C}))<y_{\rm F1}<y_{\rm G1}. \tag{C.26}$$

From (C.22) and the discussion relative to (C.19) we know $\widetilde{F}(\overline{C}_{\rm Cg}(\overline{C}_{\rm C}),y_{\rm G2})<0$ and $\widetilde{F}(\overline{C}_{\rm Cg}(\overline{C}_{\rm C}),1)<0$. If $y_*\le y_{\rm G2}$, the results from cases C1 and C2 discussed below lead to the conclusion that $\widetilde{F}(\overline{C}_{\rm Cg}(\overline{C}_{\rm C}),y)<0$ for $y\in[y_{\rm G2},1]$. However if $y_*>y_{\rm G2}$, there exists the possibility that $\widetilde{F}(\overline{C}_{\rm Cg}(\overline{C}_{\rm C}),y)$ has an even number of roots on the interval $y\in(y_{\rm G2},y_*)$. Evaluating (C.24) for parameter values typical to those in Table 1 we can demonstrate that $d\widetilde{F}(\overline{C}_{\rm Cg}(\overline{C}_{\rm C}),y)/dy<0$ for $y\in[y_{\rm G2},1]$; consequently $\widetilde{F}(\overline{C}_{\rm Cg}(\overline{C}_{\rm C}),y)$ has no zero on $y\in[y_{\rm G2},1]$. Summarizing the results on this boundary we have

$$\widetilde{F}(\overline{C}_{\rm Cg}(\overline{C}_{\rm C}),y)\begin{cases}<0, & y\in(y_{\rm F1},1],\\ =0, & y=y_{\rm F1},\\ >0, & y\in[y_{l0}(\overline{C}_{\rm Cg}(\overline{C}_{\rm C})),y_{\rm F1}).\end{cases} \tag{C.27}$$

We now consider the behavior of $\widetilde{F}(w,y)$ in the interior of Γ_{++}. We begin by explicitly isolating the w dependence of $\widetilde{F}(w,y)$. From (23a)

$$\widetilde{F}(w,y)=\overline{K}_{\rm C}\overline{C}_{\rm C}\overline{Q}+c_1(y)w+c_2(y)w^2+(\overline{\Lambda}_l f(y)+\overline{\Lambda}_{\rm g}g(y))w^3, \tag{C.28a}$$

where

$$c_1(y) = (\overline{K}_C - \overline{C}_C - 1)\overline{Q} + \overline{K}_C\overline{p}(\overline{\Lambda}_l f(y) + \overline{\Lambda}_g g(y)) + \overline{K}_C\overline{s}\overline{\Lambda}_l f(y) y^{-1/3}, \tag{C.28b}$$

$$c_2(y) = -\overline{Q} - (\overline{K}_C + \overline{p})(\overline{\Lambda}_l f(y) + \overline{\Lambda}_g g(y)) - \overline{s}\overline{\Lambda}_l f(y) y^{-1/3}. \tag{C.28c}$$

For any fixed value of $y \in (y_{l0}(\overline{C}_C), 1)$ we examine the behavior of (C.28a) as a function of w over the interval $(-\infty, \infty)$. We have

$$\lim_{w\to-\infty} \widetilde{F}(w,y) \to -\infty, \qquad \widetilde{F}(0,y) > 0, \qquad \lim_{w\to\infty} \widetilde{F}(w,y) \to \infty. \tag{C.29a}$$

From (23a) we have

$$\lim_{w\to\overline{K}_C^-} \widetilde{F}(w,y)|_{\Gamma_{++}} = -w\overline{Q} < 0. \tag{C.29b}$$

Equations (C.28a) and (C.29) specify that $\widetilde{F}(w,y)$ has three real roots, $w_1(y)$, $w_2(y)$, $w_3(y)$, where we assign $-\infty < w_1(y) < 0$ and $\overline{K}_C < w_3(y) < \infty$. Before proceeding to determine the root $w_2(y)$, we note the following lemma.

Lemma C. *$y_* > y_{F1}$, where y_* is defined in* Lemma B *and y_{F1} is defined in* (C.26).

Proof: Assume $y_* \le y_{F1}$. First consider the case $y_* < y_{F1}$. Let y be a fixed value lying in the interval (y_*, y_{F1}). By (B.18), $\widetilde{F}(w_{l0}(y), y) < 0$. We therefore conclude that the root $w_2(y)$ lies in the interval $(0, w_{l0}(y))$. However, $\widetilde{F}(\overline{C}_{Cg}(\overline{C}_C), y) > 0$ implying there is a fourth root of $\widetilde{F}(w,y)$ lying in the interval $(w_{l0}(y), \overline{C}_{Cg}(\overline{C}_C))$. Since $\widetilde{F}(w,y)$ is a polynomial of degree 3 in w, this is impossible. Therefore, the case $y_* < y_{F1}$ is untenable. For the case $y_* = y_{F1}$, $\widetilde{F}(w_*, y_*) = \widetilde{F}(\overline{C}_{Cg}(\overline{C}_C), y_{F1}) = 0$, again implying the existence of at least four real roots. Thus we conclude $y_* > y_{F1}$. ■

Note that Lemma C implies the relationship $y_{F1}(y_*)$ which must satisfy $y_{F1} \to y_{l0}(\overline{C}_C)$ as $y_* \to y_{l0}(\overline{C}_C)$ while maintaining the inequality $y_* > y_{F1}$.

In determining $w_2(y)$, we examine all possible cases on the fixed value of $y \in (y_{l0}(\overline{C}_{Cg}(\overline{C}_C)), 1)$.

Case C1. Let y lie in the interval $(y_*, 1)$. By (B.18), $\widetilde{F}(w_{l0}(y), y) < 0$ and we conclude that the root $w_2(y)$ lies in the interval $(0, w_{l0}(y))$.

Case C2. Let $y = y_*$. Then $\widetilde{F}(w_{l0}(y_*), y_*) = 0$ and we identify $w_2(y_*) = w_{l0}(y_*)$. (As noted above, if $y_* \le y_{G2}$, cases C1 and C2 lead to the conclusion that $\widetilde{F}(\overline{C}_{Cg}(\overline{C}_C), y) < 0$ for $y \in [y_{G2}, 1]$.)

Case C3. Let y lie in the interval (y_{F1}, y_*). By (B.18), $\widetilde{F}(w_{l0}(y), y) > 0$. From (C.27) $\widetilde{F}(\overline{C}_{Cg}(\overline{C}_C), y) < 0$, and we conclude $w_2(y)$ lies in the interval $(w_{l0}(y), \overline{C}_{Cg}(\overline{C}_C))$.

Case C4. Let $y = y_{F1}$. By (B.18), $\widetilde{F}(w_{l0}(y), y) > 0$. From (C.27), $\widetilde{F}(\overline{C}_{Cg}(\overline{C}_C), y_{F1}) = 0$ and we conclude $w_2(y) = \overline{C}_{Cg}(\overline{C}_C)$.

Case C5. Let y lie in the interval $(y_{l0}(\overline{C}_{Cg}(\overline{C}_C)), y_{F1})$. By (B.18), $\widetilde{F}(w_{l0}(y), y) > 0$. From (C.27), $\widetilde{F}(\overline{C}_{Cg}(\overline{C}_C), y) > 0$. Therefore, $\overline{C}_{Cg}(\overline{C}_C) < w_2(y) < \overline{K}_C$. (Note we have assigned the root $w_3(y)$ to lie in $(\overline{K}_C, \infty)$.)

Cases C1 through C5 imply that $\widetilde{F}(w,y)|_{\Gamma_{++}} = 0$ only on a curve segment $W_1(y)$ traced out by the root $w_2(y)$ for $y \in [y_*, y_{F1}]$. A sketch of $W_1(y)$, which joins the point (w_*, y_*) to $(\overline{C}_{Cg}(\overline{C}_C), y_{F1})$, is shown in Fig. 3 in the text.

Appendix D $\widetilde{F}(w,y)$ in Γ_{-+}

We address the variation of the sign of $\widetilde{F}(w,y)$ in Γ_{-+} by analyzing (23c). We start with the behavior of $\widetilde{F}(w,y)$ on the boundaries of Γ_{-+}. On the boundary $y = 0$, $w \in [\overline{p}, \overline{C}_{Cg}(\overline{C}_C)]$,

$$\lim_{y\to0^+} \widetilde{F}(w,y) \to \overline{\Lambda}_l\overline{s}(\overline{K}_C - w)F_2(w)y^{-1/3} \to -\infty. \tag{D.30}$$

From (23d) and restriction (24) we have demonstrated in the paper that $\widetilde{F}(w,y) < 0$ on the boundary Γ_{g0}. On the boundary $y = 1$, $w \in [\overline{p}, \overline{p} + \overline{s}]$,

$$\widetilde{F}(w,1) = \overline{K}_C\overline{C}_C\overline{Q} + d_1 w + d_2 w^2 + (\overline{\Lambda}_l + \overline{\Lambda}_g)w^3, \tag{D.31}$$

where

$$d_1 = -(1 - \overline{K}_C + \overline{C}_C)\overline{Q} - \overline{\Lambda}_l(1 - \overline{K}_C)(\overline{p} + \overline{s}) + \overline{\Lambda}_g\overline{K}_C\overline{p},$$

$$d_2 = -\overline{Q} + \overline{\Lambda}_l(1 - \overline{K}_C - \overline{p} - \overline{s}) - \overline{\Lambda}_g(\overline{K}_C + \overline{p}).$$

Considering (D.31) as a function of w on $(-\infty,\infty)$ we note

$$\begin{array}{lll} \lim_{w\to-\infty}\widetilde{F}(w,1)\to-\infty, & \lim_{w\to\infty}\widetilde{F}(w,1)\to\infty, & \\ \widetilde{F}(0,1)>0, & \widetilde{F}(\overline{p},1)<0, & \widetilde{F}(\overline{p}+\overline{s},1)<0. \end{array} \tag{D.32}$$

The last two inequalities in (D.32) follow from (24). Equations (D.32) imply that $\widetilde{F}(w,1)$ has exactly three real roots, w_1, w_2, w_3, satisfying $w_1<0<w_2<\overline{p}<\overline{p}+\overline{s}<w_3$. We therefore conclude $\widetilde{F}(w,1)<0$ on $[\overline{p},\overline{p}+\overline{s}]$.

The behavior of $\widetilde{F}(w,y)$ on the boundary Γ_{l0} was analyzed in Appendix B. For the boundary segment $w=\overline{C}_{\rm Cg}(\overline{C}_{\rm C})$, $y\in(0,y_{l0}(\overline{C}_{\rm Cg}(\overline{C}_{\rm C})))$, we know $\widetilde{F}(\overline{C}_{\rm Cg}(\overline{C}_{\rm C}),y_{l0}(\overline{C}_{\rm Cg}(\overline{C}_{\rm C})))>0$ while $\lim_{y\to0^+}\widetilde{F}(\overline{C}_{\rm Cg}(\overline{C}_{\rm C}),y)\to-\infty$. Thus, there exists at least one point $y_{\rm F2}$ on this boundary interval such that $\widetilde{F}(\overline{C}_{\rm Cg}(\overline{C}_{\rm C}),y_{\rm F2})=0$. We assert here that $y_{\rm F2}\in(0,y_{l0}(\overline{C}_{\rm Cg}(\overline{C}_{\rm C})))$ is a unique value on this boundary interval satisfying

$$\widetilde{F}(\overline{C}_{\rm Cg}(\overline{C}_{\rm C}),y)\begin{cases} >0, & y\in(y_{\rm F2},y_{l0}(\overline{C}_{\rm Cg}(\overline{C}_{\rm C}))),\\ =0, & y=y_{\rm F2},\\ <0, & y\in(0,y_{\rm F2}). \end{cases} \tag{D.33}$$

This assertion is proven below as part of the analysis (cases DI and DII) on the dependence of $\widetilde{F}(w,y)|_{\Gamma_{-+}}$ on y.

We consider the behavior of $\widetilde{F}(w,y)|_{\Gamma_{-+}}$ in the interior of Γ_{-+} by first examing its dependence along lines of constant y. From (23c),

$$\widetilde{F}(w,y)=\overline{K}_{\rm C}\overline{C}_{\rm C}\overline{Q}+d_1(y)w+d_2(y)w^2+(\overline{\Lambda}_l+\overline{\Lambda}_{\rm g}g(y))w^3, \tag{D.34a}$$

where

$$d_1=c_1(y)|_{f(y)=1}-\overline{\Lambda}_l\left(\overline{p}+\overline{s}y^{-1/3}\right),\qquad d_2(y)=c_2(y)|_{f(y)=1}+\overline{\Lambda}_l, \tag{D.34b}$$

with $c_1(y)$, $c_2(y)$ given by (C.28). We examine all possible cases (labelled D0a-f) on the fixed value of $y\in(0,1)$.

D0a: For any fixed value $y_1\in(y_*,1)$, from (D.34a),

$$\begin{array}{lll} \lim_{w\to-\infty}\widetilde{F}(w,y_1)\to-\infty, & \lim_{w\to\infty}\widetilde{F}(w,y_1)\to\infty, & \\ \widetilde{F}(0,y_1)>0 & \widetilde{F}(\overline{p},y_1)<0, & \widetilde{F}(w_{l0}(y_1),y_1)<0. \end{array} \tag{D.35}$$

Equations (D.34a) and (D.35) specify that $\widetilde{F}(w,y_1)$ has only three real roots, $w_1(y_1)$, $w_2(y_1)$, $w_3(y_1)$, where $w_1(y_1)<0<w_2(y_1)<\overline{p}$ and $w_{l0}(y_1)<w_3(y_1)$. Thus $\widetilde{F}(w,y_1)\neq0$ for any $(w,y_1>y_*)\in\Gamma_{-+}$.

D0b: If $y_1=y_*$, then (D.35) holds with the last equation changed to $\widetilde{F}(w_*,y_*)=0$ and we conclude the third real root satisfies $w_3(y_1)=w_*$.

D0c: If $y_1\in[y_{l0}(\overline{C}_{\rm Cg}(\overline{C}_{\rm C})),y_*)$, then (D.35) holds with the last equation changed to $\widetilde{F}(w_{l0}(y_1),y_1)>0$ and we conclude $\overline{p}<w_3(y_1)<w_{l0}(y_1)$.

D0d: If $y_1\in(y_{\rm F2},y_{l0}(\overline{C}_{\rm Cg}(\overline{C}_{\rm C})))$, then (D.35) holds with the last equation changed to $\widetilde{F}(\overline{C}_{\rm Cg}(\overline{C}_{\rm C}),y_1)>0$ and we conclude $\overline{p}<w_3(y_1)<\overline{C}_{\rm Cg}(\overline{C}_{\rm C})$.

D0e: If $y_1=y_{\rm F2}$, then (D.35) holds with the last equation changed to $\widetilde{F}(\overline{C}_{\rm Cg}(\overline{C}_{\rm C}),y_1)=0$ and we conclude $w_3(y_1)=\overline{C}_{\rm Cg}(\overline{C}_{\rm C})$.

D0f: If $y_1\in(0,y_{\rm F2})$, then (D.35) holds with the last equation changed to $\widetilde{F}(\overline{C}_{\rm Cg}(\overline{C}_{\rm C}),y_1)<0$ and we conclude $\overline{C}_{\rm Cg}(\overline{C}_{\rm C})<w_3(y_1)$.

Thus $\widetilde{F}(w,y_1)\neq0$ for any point $(w,y_1<y_{\rm F2})\in\Gamma_{-+}$.

As $\widetilde{F}(w,y)|_{\Gamma_{-+}}$ is a continuous function in both of its variables, cases D0a through D0f imply that $\widetilde{F}(w,y)|_{\Gamma_{-+}}=0$ only on a continuous curve segment $W_2(y)$ traced out by the root $w_3(y)$ for $y\in[y_{\rm F2},y_*]$. $W_2(y)$ joins the point (w_*,y_*) to the point $(\overline{C}_{\rm Cg}(\overline{C}_{\rm C}),y_{\rm F2})$. Note $W_2(y)$ is a single-valued function of y.

To further explore the behavior of the curve $W_2(y)$ we examine the y-dependence of $\widetilde{F}(w,y)|_{\Gamma_{-+}}$ along lines of constant w. From (23c) the first two partial derivatives of $\widetilde{F}(w,y)|_{\Gamma_{-+}}$ with respect to y are

$$\frac{\partial\widetilde{F}(w,y)}{\partial y}=(\overline{K}_{\rm C}-w)\left\{-F_2(w)\frac{\overline{\Lambda}_l\overline{s}}{3y^{4/3}}-3\overline{\Lambda}_{\rm g}w(w-\overline{p})y^2\right\}, \tag{D.36a}$$

$$\frac{\partial^2\widetilde{F}(w,y)}{\partial y^2}=(\overline{K}_{\rm C}-w)\left\{F_2(w)\frac{4\overline{\Lambda}_l\overline{s}}{9y^{7/3}}-6\overline{\Lambda}_{\rm g}w(w-\overline{p})y\right\}<0. \tag{D.36b}$$

In obtaining the inequality in (D.36b), recall that $F_2(w) < 0$. For any fixed value of $w \in (\overline{p}, \overline{C}_{Cg}(\overline{C}_C)]$, $\widetilde{F}(w,y)|_{\Gamma_{-+}}$ is concave down having maximum value at $y_{\max}(w)$ where the first partial, $(\partial \widetilde{F}(w,y)/\partial y$, vanishes. From (D.36a), $y_{\max}(w)$ satisfies

$$(y_{\max}(w))^{10/3} = \frac{-F_2(w)\bar{s}\delta}{w(w-\overline{p})} = \frac{\bar{s}\delta[1-(\overline{K}_C - w)]}{(w-\overline{p})(\overline{K}_C - w)}, \qquad \overline{p} < w < \overline{K}_C, \tag{D.37}$$

where $\delta \equiv \overline{\Lambda}_l/(9\overline{\Lambda}_g)$. Note, $y_{\max}(w) > 0$ for $w \in (\overline{p}, \overline{K}_C)$. As a function of w, the curve (D.37) has the following limits: $\lim_{w\to\overline{p}^+} y_{\max}(w) \to \infty$ and $\lim_{w\to\overline{K}_C^-} y_{\max}(w) \to \infty$. From (D.37), $y_{\max}(w) = 1$ at two values, $\widehat{w}_\pm$, satisfying the quadratic

$$\widehat{w}_\pm^2 - (\overline{K}_C + \overline{p} - \bar{s}\delta)\widehat{w}_\pm + \overline{K}_c\overline{p} + \bar{s}\delta(1-\overline{K}_C) = 0.$$

Assuming (see e.g. Table 1) that $4\bar{s}\delta \ll (\overline{K}_C + \overline{p} - \bar{s}\delta)^2$, to first order in a Taylor expansion of the square root in the quadratic formula solution we have,

$$\widehat{w}_\pm \cong \frac{1}{2}\left\{(\overline{K}_C + \overline{p} - \bar{s}\delta) \pm (\overline{K}_C - \overline{p} + \bar{s}\delta)\left[1 - \frac{2\bar{s}\delta}{(\overline{K}_C - \overline{p} + \bar{s}\delta)^2}\right]\right\}.$$

Evaluating these two values we see

$$\widehat{w}_- \cong \overline{p} + \bar{s}\delta\frac{1-(\overline{K}_C - \overline{p} + \bar{s}\delta)}{\overline{K}_C - \overline{p} + \bar{s}\delta} \gtrsim \overline{p}, \quad \widehat{w}_+ \cong \overline{K}_C - \frac{\bar{s}\delta}{\overline{K}_C - \overline{p} + \bar{s}\delta} \lesssim \overline{K}_C.$$

Thus only $\widehat{w}_-$ lies in the region Γ_{-+}. We rename this value as $\widehat{w}_- \stackrel{\text{def}}{=} \widehat{w}_1$.

We next consider the local extremum values of the curve $y_{\max}(w)$ at which

$$\frac{dy_{\max}(w)}{dw} = \frac{3}{10}[y_{\max}(w)]^{-7/3}\,\bar{s}\delta\frac{[(\overline{K}_C - w)^2 + 2w - \overline{K}_C - \overline{p}]}{(\overline{K}_C - w)^2\,(w-\overline{p})^2} = 0.$$

The extrema occur at two values $\breve{w}_\pm$ satisfying $(\overline{K}_C - \breve{w}_\pm)^2 - 2(\overline{K}_C - \breve{w}_\pm) + \overline{K}_C - \overline{p} = 0$, i.e. $\breve{w}_\pm = \overline{p} - (1 - \overline{K}_C + \overline{p}) \pm (1 - \overline{K}_C + \overline{p})^{1/2}$. Noting that $\overline{p} < \overline{K}_C < 1$, we have $1 > (1-\overline{K}_C + \overline{p})^{1/2} > (1 - \overline{K}_C + \overline{p})$. Therefore the root $\breve{w}_- < \overline{p}$ lies outside the range of interest $w \in [\overline{p}, \overline{C}_{Cg}(\overline{C}_C)]$ and the desired root is $\breve{w}_+ > \overline{p}$. For notational consistency we rename this value $\breve{w}_+ \stackrel{\text{def}}{=} \widehat{w}_0$. At $\widehat{w}_0$, the curve $y_{\max}(w)$ achieves a minimum y-value. It is not guaranteed that the point $(\widehat{w}_0, y_{\max}(\widehat{w}_0))$ lies in the region Γ_{-+}; in fact for the values in Table 1, $\overline{C}_{Cg}(\overline{C}_C) < \widehat{w}_0 < \overline{K}_C$. Evaluated using parameter values from Table 1, the segment of the curve $y_{\max}(w)$ lying in Γ_{-+} is plotted in Fig. 3.

We now consider the crossing point (w_Γ, y_Γ) of the curves $y_{\max}(w)$ and $y_{l0}(w)$. From (26) and (D.37), w_Γ satisfies

$$U_\Gamma^9(U_\Gamma - \Delta + 1) + \bar{s}^9(U_\Gamma - \Delta)/\delta = 0, \tag{D.38}$$

where $U_\Gamma = w_\Gamma - \overline{p}$, $\Delta = \overline{K}_C - \overline{p}$.

Lemma D. *Equation (D.38) has a single solution $U_\Gamma \in [0,\Delta]$ (i.e. $w_\Gamma \in [\overline{p}, \overline{K}_C]$). In particular, $U_\Gamma \cong (1+\varepsilon)\bar{s}$ where $\varepsilon < 10^{-1}$.*

Proof: Let $h(U)$ denote the function

$$h(U) = U^9(U + 1 - \Delta) + \frac{\bar{s}^9(U-\Delta)}{\delta}.$$

We are only interested in the range $U \in [0,\Delta]$. Noting that

$$h(0) = -\frac{\bar{s}^9\Delta}{\delta} < 0, \qquad h(\Delta) = \Delta^9 > 0,$$

$$h'(U) = U^8[10U + 9(1-\Delta)] + \frac{\bar{s}^9}{\delta}, \qquad h''(U) = 9U^7[10U + 8(1-\Delta)] > 0,$$

we see that $h'(U) > 0$ on $[0,\Delta]$ and conclude that $h(U) = 0$ for a single $U_\Gamma \in [0,\Delta]$. Substituting $U_\Gamma \cong (1+\varepsilon)\bar{s}$ into (D.38), to first order in a Taylor expansion in ε (assumed small) we find

$$\varepsilon = \frac{1 - (1+\delta)(\bar{s} + 1 - \Delta)}{(1+10\delta)\bar{s} + 9\delta(1-\Delta)}.$$

Using parameter values from Table 1 we have $\varepsilon \approx 0.094$. Using a second order Taylor expansion yields $\varepsilon \approx 0.071$. ■

From Lemma D we conclude the curve $y_{\max}(w)$ crosses Γ_{l0} at the single point w_Γ, y_Γ where

$$\overline{p}+\overline{s} \lesssim w_\Gamma = \overline{p}+(1+\varepsilon)\overline{s} < \overline{C}_{\rm Cg}(\overline{C}_{\rm C}), \qquad y_\Gamma = \left[\frac{\overline{s}}{w_\Gamma-\overline{p}}\right]^3 = (1+\varepsilon)^{-3}.$$

This crossing point is also shown in Fig. 3.

The behavior of $W_2(y)$ depends on two cases, DI: $w_\Gamma \le w_*$ or DII: $w_\Gamma > w_*$.

Case DI: $w_\Gamma \le w_*$. We examine all possible values of w.

DIa: Let $w \in (\overline{p}, \widehat{w}_1)$. Since $\widetilde{F}(w,0) \to -\infty$, $\widetilde{F}(w,1) < 0$ and $\partial \widetilde{F}(w,y)/\partial y > 0$, we conclude $\widetilde{F}(w,y)|_{\Gamma_{-+}} < 0$ for $w \in (\overline{p}, \widehat{w}_1)$.

DIb: Let $w = \widehat{w}_1$. Since $\widetilde{F}(\widehat{w}_1,0) \to -\infty$, $\widetilde{F}(\widehat{w}_1,1) < 0$ and $\partial \widetilde{F}(w,y)/\partial y|_{\widehat{w}_1} > 0$ for $0 < y < 1$, we conclude $\widetilde{F}(\widehat{w}_1,y)|_{\Gamma_{-+}} < 0$.

DIc: $w \in (\widehat{w}_1, w_\Gamma)$. For any w in this range, $\widetilde{F}(w,y)$ goes through a maximum value at $y_{\max}(w)$. While $\widetilde{F}(w,y) < 0$ near the boundaries $y = 0$ and $y = \min(1, y_{l0}(w))$, it is possible that $\widetilde{F}(w, y_{\max}(w)) \ge 0$. Thus for $w \in (\widehat{w}_1, w_\Gamma)$, $\widetilde{F}(w_\Gamma, y)|_{\Gamma_{-+}}$ may have: i) no real roots, ii) one real root $y(w) = y_{\max}(w)$, or iii) two real roots $y_1(w)$, $y_2(w)$ satisfying $0 < y_1(w) < y_{\max}(w) < y_2(w) < \min(1, y_{l0}(w))$.

DId: $w = w_\Gamma$. This case is similar to DIb with the upper boundary value being $y_{l0}(w_\Gamma)$. Thus $\widetilde{F}(w_\Gamma, y)|_{\Gamma_{-+}} < 0$.

DIe: $w \in (w_\Gamma, w_*)$. This case is similar to DIa with the upper boundary value being $y_{l0}(w)$. Thus $\widetilde{F}(w,y)|_{\Gamma_{-+}} < 0$.

DIf: $w = w_*$. $\widetilde{F}(w_*, y)|_{\Gamma_{-+}}$ has one real root at the point (w_*, y_*).

DIg: $w \in (w_*, \overline{C}_{\rm Cg}(\overline{C}_{\rm C})]$. Here $\lim_{y\to 0^+} \widetilde{F}(w,y) \to -\infty$ and $\widetilde{F}(w, y_{l0}(w)) > 0$. Since $\partial \widetilde{F}(w,y)/\partial y > 0$ on $0 < y < y_{l0}(w)$, we conclude $\widetilde{F}(w,y)|_{\Gamma_{-+}}$ has a single real zero, $y_1(w)$, satisfying $0 < y_1(w) < y_{l0}(w)$.

Cases DIf and DIg show that $\widetilde{F}(w,y)|_{\Gamma_{-+}} = 0$ only on a curve segment traced out by the root $y_1(w)$ for $w \in [w_*, \overline{C}_{\rm Cg}(\overline{C}_{\rm C})]$. Since DIe states that $\widetilde{F}(w,y)|_{\Gamma_{-+}} \ne 0$ for $w \in (w_\Gamma, w_*)$, we conclude that: 1) the curve segment identified in DIf and DIg is uniquely the continuous curve segment $W_2(y)$ identified previously, and 2) case DIc can only support the conclusion $\widetilde{F}(w,y) < 0$ for $w \in (\widehat{w}_1, w_\Gamma)$. Combining the results of D0 and DI, we have verified that $W_2(y)$ connects (w_*, y_*) to $(\overline{C}_{\rm Cg}(\overline{C}_{\rm C}), y_{\rm F1})$ and $W_2(y)$ is a continuous, one-to-one, onto map, $[w_*, \overline{C}_{\rm Cg}(\overline{C}_{\rm C})] \leftrightarrow [y_*, y_{\rm F2}]$. The form of the curve $W_2(y)$ for case DI is sketched in Fig. 3.

Case DII: $w_\Gamma > w_*$. As in case DI, we examine all possible values of w. As the arguments are generally similar to case DI, we shorten the presentation for each case.

Cases DIIa and **DIIb** are identical to DIa and DIb respectively.

DIIc: $w \in (\widehat{w}_1, w_*)$. For each w in this range, $\widetilde{F}(w_\Gamma, y)|_{\Gamma_{-+}}$ can have: i) no real roots, ii) one real root $y_1(w) = y_{\max}(w)$, or iii) two real roots $y_1(w)$, $y_2(w)$ satisfying $0 < y_1(w) < y_{\max}(w) < y_2(w) < \min(1, y_{l0}(w))$.

DIId: $w = w_*$. As $\widetilde{F}(w_*, y_{\max}(w_*)) > \widetilde{F}(w_*, y_*) = 0$ then $\widetilde{F}(w_*, y)|_{\Gamma_{-+}}$ has exactly two real roots $y_1(w_*)$, $y_2(w_*)$ satisfying $0 < y_1(w_*) < y_{\max}(w_*) < y_2(w_*) = y_*$.

DIIe: $w \in (w_*, w_\Gamma)$. This case is similar to DIg. Thus $\widetilde{F}(w,y)|_{\Gamma_{-+}}$ has a single real zero $y_1(w)$ satisfying $0 < y_1(w) < y_{l0}(w)$.

DIIf: $w \in [w_\Gamma, \overline{C}_{\rm Cg}(\overline{C}_{\rm C})]$. The argument follows DIg; we conclude $\widetilde{F}(w,y)|_{\Gamma_{-+}}$ has a single real zero, $y_1(w)$, satisfying $0 < y_1(w) < y_{l0}(w)$.

The curve traced out by the root $y_1(w)$ in cases DIIa through DIIf must accord with the curve $W_2(y)$ on which $\widetilde{F}(w,y)|_{\Gamma_{-+}} = 0$. We therefore conclude that case DIIc must read:

DIIc′ $w \in (\widehat{w}_1, w_*)$. There exists $w_m \in (\widehat{w}_1, w_*)$ such that: for any $w \in (\widehat{w}_1, w_m)$, $\widetilde{F}(w,y)|_{\Gamma_{-+}}$ has no real roots; for $w = w_m$, $\widetilde{F}(w,y)|_{\Gamma_{-+}}$ has one real root $y_m = y_{\max}(w_m)$; and for any $w \in (w_m, w_*)$, $\widetilde{F}(w,y)|_{\Gamma_{-+}}$ has two real roots $y_1(w)$, $y_2(w)$ satisfying $0 < y_1(w) < y_{\max}(w) < y_2(w) < y_*$. Combined with the results from cases D0, we have that on $[y_{\rm F2}, y_m]$, $W_2(y)$ strictly decreases in value from $\overline{C}_{\rm Cg}(\overline{C}_{\rm C})$ to w_m, and on $[y_m, y_*]$, $W_2(y)$ strictly increases in value from w_m to w_*.The form for the curve $W_2(y)$ in DII and the point (w_m, y_m) are illustrated in Fig. 3.

Finally we note that cases DIg and DIIf show the existence of a single root of $\widetilde{F}(w,y)|_{\Gamma_{-+}}$ on the boundary segment $w = \overline{C}_{\rm Cg}(\overline{C}_{\rm C})$, $y \in (0, y_{l0}(\overline{C}_{\rm Cg}(\overline{C}_{\rm C})))$. This root is the unique point $(\overline{C}_{\rm Cg}(\overline{C}_{\rm C}), y_{\rm F2})$ claimed in (D.33).

Appendix E $\widetilde{F}(w,y)$ in Γ_{--}

We address the variation of the sign of $\tilde{F}(w,y)$ in Γ_{--} by analyzing (23e). We start with the behavior of $\widetilde{F}(w,y)$ on the boundaries of Γ_{--}. From (23d) and restriction (24) we have demonstrated in the paper that $\widetilde{F}(w,y)|_{\Gamma_{\rm g0}} = \widetilde{F}(\overline{p},y) < 0$. On the boundary $y = 0$, $w \in [0, \overline{p})$ we have $\lim_{y\to 0^+} \widetilde{F}(w,y) \to -\infty$. From (23e) it is straightforward to check that $\widetilde{F}(0,y) = \overline{K}_{\rm C}\overline{C}_{\rm C}\overline{Q} > 0$. The behavior of $\widetilde{F}(w,y)|_{\Gamma_{--}}$ on the boundary $y = 1$, $w \in [0, \overline{p}]$ can be determined by examining the behavior of $\widetilde{F}(w,1)|_{\Gamma_{--}}$ with respect to w. From (23e) we can write

$$\widetilde{F}(w,y) = \overline{K}_{\rm C}\overline{C}_{\rm C}\overline{Q} + e_1(y)w + e_2(y)w^2 + \overline{\Lambda}_l w^3, \tag{E.40}$$

where $e_1(y) = d_1(y)|_{g(y)=0}$ and $e_2(y) = d_2(y)|_{g(y)=0}$. From (E.40) we have the following properties

$$\begin{aligned} &\lim_{w\to-\infty} \widetilde{F}(w,1) \to -\infty, && \widetilde{F}(0,1) > 0, \\ &\widetilde{F}(\overline{p},1) < 0 \text{ by (24)}, && \lim_{w\to\infty} \widetilde{F}(w,1) \to \infty. \end{aligned} \tag{E.41}$$

Equations (E.40) and (E.41) imply that $\widetilde{F}(w,1)$ has three real roots, w_1, w_2, w_3, satisfying $w_1 < 0 < w_2 < \overline{p} < w_3$. Let $w_2 \overset{\text{def}}{=} w_{F3}$. Then we have

$$\widetilde{F}(w,1) > 0, \quad w \in [0, w_{F_3}), \qquad \widetilde{F}(w,1) < 0, \quad w \in (w_{F3}, \overline{p}]. \tag{E.42}$$

With the behavior of $\widetilde{F}(w,y)|_{\Gamma_{--}}$ determined on the boundaries, we now consider its behavior in the interior. From (23e), $\widetilde{F}(w,y)$ can be written

$$\widetilde{F}(w,y) = E_0(w) + E_1(w) y^{-1/3}, \tag{E.43}$$

where $E_1(w) = -w\overline{\Lambda}_l \overline{p}(1 - \overline{K}_C + w) < 0$. The first two partials of $\widetilde{F}(w,y)$ with respect to y are

$$\frac{\partial \widetilde{F}(w,y)}{\partial y} = -\frac{1}{3} E_1(w) y^{-4/3} > 0, \qquad \frac{\partial^2 \widetilde{F}(w,y)}{\partial y^2} = \frac{4}{9} E_1(w) y^{-7/3} < 0. \tag{E.44}$$

From (E.42) and (E.44) we conclude the following.
i) For each fixed $w \in (0, w_{F3}]$, $\widetilde{F}(w,y) = 0$ at exactly one value $y = Y_3(w)$, with $Y_3(w_{F3}) = 1$. For $y \in (0, Y_3(w))$, $\widetilde{F}(w,y) < 0$ and for $y \in (Y_3(w), 1)$, $\widetilde{F}(w,y) > 0$.
ii) For each fixed $w \in (w_{F3}, \overline{p}]$, $\widetilde{F}(w,y) < 0$.
From i) and ii) we have the existence of the curve $Y_3(w)$ along which $\widetilde{F}(w, Y_3(w)) = 0$. From (E.43), $Y_3(w)$ has the explicit form $Y_3(w) = (-E_1(w)/E_0(w))^3$ satisfying $\lim_{w\to 0^+} Y_3(w) = 0$.

As $\widetilde{F}(w, Y_3(w)) = 0$, we can compute an expression for the slope of $Y_3(w)$ from (E.43),

$$\begin{aligned} 0 &= \frac{dE_0(w)}{dw} + \frac{dE_1(w)}{dw} Y_3(w)^{-1/3} - \frac{1}{3} E_1(w) Y_3(w)^{-4/3} \left(\frac{dY_3(w)}{dw} \right), \\ &= \left. \frac{\partial \widetilde{F}(w,y)}{\partial w} \right|_{Y_3(w)} + \left. \frac{\partial \widetilde{F}(w,y)}{\partial y} \right|_{Y_3(w)} \frac{dY_3(w)}{dw}, \\ \to \frac{dY_3(w)}{dw} &= - \left. \frac{\partial \widetilde{F}(w,y)}{\partial w} \right|_{Y_3(w)} \Bigg/ \left. \frac{\partial \widetilde{F}(w,y)}{\partial y} \right|_{Y_3(w)}. \end{aligned} \tag{E.45}$$

From i) we know that $Y_3(w)$ maps the interval $w \in (0, w_{F3}]$ onto $y \in (0,1]$ in a one-to-one fashion. Therefore $Y_3(w)$ implicitly defines the inverse curve $W_3(y)$ which maps $y \in (0,1]$ onto $w \in (0, w_{F3}]$ in a one-to-one fashion with $\lim_{y\to 0^+} W_3(y) = 0$ and $W_3(1) = w_{F3}$. As $W_3(y)$ is the only curve on which $\widetilde{F}(w,y)|_{\Gamma_{--}} = 0$, for each fixed $y \in (0,1]$ we have $\widetilde{F}(w,y) > 0$ for $w \in (0, W_3(y))$, and $\widetilde{F}(w,y) < 0$ for $w \in (W_3(y), \overline{p}]$. Thus we conclude $\partial \widetilde{F}(w,y)/\partial w|_{Y_3(w)} < 0$. By (E.44) we know $\partial \widetilde{F}(w,y)/\partial y|_{Y_3(w)} > 0$. Applied to (E.45), these observations lead to the conclusion, $dY_3(w)/dw > 0$. The curve $W_3(y)$ is sketched in Fig. 3.

Appendix F Initial conditions for gas bubble formation

As noted in the discussion of solution trajectories in the paper, initial bubble size is determined by microscopic, non-linear dynamics at a nucleation site. To mimic this, we set the initial bubble radius equal to the radius value of the inlet. Thus,

$$y_0 = (a/\mathrm{R}_{\text{pore}})^3. \tag{F.46}$$

To determine initial bubble CO_2 concentration, we assume that the pressure in the liquid phase does not change at the moment of bubble formation. From (14′) this assumption gives $\overline{p}_l^{\text{sp}} = \overline{p}_g - \overline{p}_c = w_0 - \bar{s} y_0^{-1/3}$. Using (2) we derive a value for w_0,

$$w_0 = \overline{p} + \bar{s} y_0^{-\frac{1}{3}} + \overline{Q}/\overline{\Lambda}_l = w_{lo}(y_0) + \overline{Q}/\overline{\Lambda}_l. \tag{F.47}$$

Finally, we impose mass conservation at the time of bubble formation; the loss of CO_2 in the liquid phase must equal the amount of CO_2 in the gas bubble. (This is consistent with our previous assumption that phase changes occur faster than flow rates.) Using the two-phase flow relation (13) between $\overline{C}_{Cl}$ and $w = \overline{C}_{Cg}$, CO_2 conservation gives

$$\overline{C}_{Cl}^{sp}(t_b) - \frac{w_0}{\overline{K}_C - w_0}(1 - y_0) = w_0 y_0, \tag{F.48a}$$

where $\overline{C}_{Cl}^{sp}(t_b)$ denotes the CO_2 concentration in the liquid just prior to bubble formation at time t_b. Using (2), (F.48a) can be used to solve for t_b,

$$t_b = -\frac{1}{\overline{Q}} \ln\left\{1 - \frac{1}{\overline{C}_C}\left(\frac{w_0}{\overline{K}_C - w_0}\right)[1 - (1 + w_0 - \overline{K}_C)y_0]\right\}. \tag{F.48b}$$

Appendix G

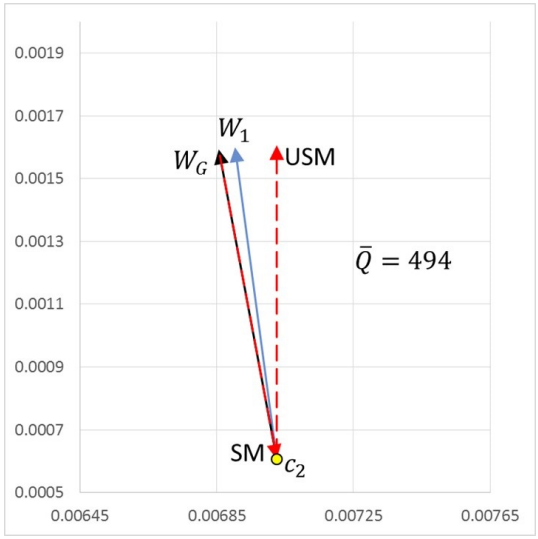

Figure G. Properly scaled figure showing directions at the critical point c_2. The red arrow labeled USM corresponds to the direction of the unstable manifold and the red arrow labeled SM is the direction of the stable manifold. Also noted (black, blue arrows) are the directions of the curves and W_G and W_1 at c_2. The direction of W_G is almost antiparallel to that of the stable manifold.

Appendix H

Assumptions used in analysis of the dynamical system (18′)
The liquid phase is incompressible
The concentration of water in the liquid phase, C_W, is constant
The outlet reservoir remains pure water
Phase changes occur more rapidly than fluid transport
The liquid phase is perfectly wetting
Any gas phase forming in a pore occurs as a single bubble
The gas phase acts as an ideal gas
The thermodynamic values $\overline{K}_H(T)$ and $\overline{K}_C(T)$ satisfy $\overline{K}_H(T)/\overline{K}_C(T) \approx 0$ implying that the concentration of H_2O in the gas phase is negligible, $\overline{C}_{Hg}(w) \approx 0$
$w \gg \overline{K}_H(T) = O(10^{-5})$
The flow rate, $\overline{Q}$, is restricted to the range given by equation (24)

Bubble initial conditions: initial bubble radius equals inlet radius liquid pressure does not change at moment of bubble formation

$4\overline{K}_{\mathrm{C}}/(1+\overline{C}_{\mathrm{C}}+\overline{K}_{\mathrm{C}})^{2} \ll 1$

$\widetilde{F}(\overline{C}_{\mathrm{Cg}}(\overline{C}_{\mathrm{C}}),y)$ has no zero on the interval $y \in (y_{G2}, y_{*})$ when $y_{*} > y_{G2}$

$4\bar{s}\delta \ll (\overline{K}_{\mathrm{C}}+\overline{p}+\bar{s}\delta)^{2}$ where $\delta = \overline{\Lambda}_{l}/(9\overline{\Lambda}_{\mathrm{g}})$